

Muon $g-2$, Dark Matter and the Higgs mass in No-Scale Supergravity

Adam K. Forster* ¹ and Stephen F. King* ²

* *Department of Physics and Astronomy, University of Southampton,
SO17 1BJ Southampton, United Kingdom*

Abstract

We discuss the phenomenology of no-scale supergravity (SUGRA), in which the universal scalar mass is zero at the high scale, focussing on the recently updated muon $g-2$ measurement, and including dark matter and the correct Higgs boson mass. Such no-scale supergravity scenarios arise naturally from string theory and are also inspired by the successful Starobinsky inflation, with a class of minimal models leading to a strict upper bound on the gravitino mass $m_{3/2} < 10^3$ TeV. We perform a Monte Carlo scan over the allowed parameter space, assuming a mixture of pure gravity mediated and universal gaugino masses, using the SPheno package linked to FeynHiggs, MicrOmegas and CheckMate, displaying the results in terms of a Likelihood function. We present results for zero and non-zero trilinear soft parameters, and for different signs of gaugino masses, giving a representative set of benchmark points for each viable region of parameter space. We find that, while no-scale SUGRA can readily satisfy the dark matter and Higgs boson mass requirements, consistent with all other phenomenological constraints, the muon $g-2$ measurement may be accommodated only in certain regions of parameter space, close to the LHC excluded regions for light sleptons and charginos.

¹E-mail: A.K.Forster@soton.ac.uk

²E-mail: king@soton.ac.uk

Contents

1	Introduction	1
2	The no-scale SUGRA model parameters	4
3	Method	5
4	No-scale SUGRA with $A_0 = 0$ (Case I)	7
4.1	Positive k (Scan 1)	8
4.2	Negative k (Scan 2)	22
5	No-scale SUGRA with non-zero A_0 (Case II)	29
5.1	Positive k (Scan 3)	29
5.2	Negative k (Scan 4)	30
6	Conclusion	39
7	Acknowledgments	40

1 Introduction

Recent experimental results have propelled the anomalous muon magnetic moment $g - 2$ back into the centre stage of particle physics. Following the original Brookhaven National Laboratory measurements [1], the Fermilab Muon collaboration has recently affirmed these findings [2], with the combined results now showing a 4.2σ discrepancy with the Standard Model (SM) calculation [3–23],

$$a_\mu^{EXP} - a_\mu^{SM} = (2.51 \pm 0.59) \times 10^{-9} \quad (1)$$

where $a_\mu = \frac{g-2}{2}$. One of the classic explanations of the discrepancy is provided by supersymmetry (SUSY), due to loops of light sleptons, $\tilde{\mu}$, $\tilde{\nu}_\mu$, and light electroweak gauginos [24]. These days such an explanation must be made consistent with the measurement of the Higgs boson mass, and LHC constraints on superpartners, both of which point towards rather heavy squarks and gluinos, and such studies have been recently performed in various SUSY models [25–32].

Here we shall be interested in the phenomenology of no-scale supergravity (SUGRA) (for a review and early references see [33]), focussing on the interplay between the muon $g-2$, dark matter and the Higgs boson mass in particular. No-scale SUGRA is an ultraviolet (UV) completion of the minimal supersymmetric standard model (MSSM), in which the scalar masses are zero at the high scale and are subsequently generated by renormalisation group (RG) running via couplings to the non-zero gaugino masses. Apart from its minimality, it is motivated by string theory and more recently by the fact that the hidden sector contains the ingredients for inflation. However, its phenomenological viability is not straightforward, given the fact the Higgs mass requires large stop masses, while the muon $g-2$ requires light slepton masses, and dark matter is known to be non-trivial to achieve in the general MSSM, and all this must be achieved in no-scale SUGRA starting from zero scalar masses at the high scale. This provides the main motivation for a detailed phenomenological study of no-scale SUGRA. In our approach, there will be an important constraint coming from inflation, to which we now turn.

The idea of inflation is one of the key concepts in modern cosmology [34–39]. Not only does it explain the vast size of the universe (the flatness problem), it also explains the extreme homogeneity and isotropy of the universe on cosmological scales (the horizon problem), as well as diluting cosmological relics (the monopole problem). Furthermore, the slow rolling inflaton provides small quantum fluctuations which eventually lead to large scale structure [40, 41]. However, despite its successes, the precise mechanism that causes inflation is unknown. Clues to the theory behind inflation, may come from current observational data [42], where the spectral index is measured to be $n_s \approx 0.96 \pm 0.007$ with a low tensor-to-scalar ratio $r < 0.08$. These data exclude the simplest chaotic models with inflaton potentials ϕ^2 or ϕ^4 [43]. Amongst the successful models which are consistent with these data is Starobinsky inflation [36, 44], which may have a link to SUSY models [45–47]. Since inflation is sensitive to ultraviolet (UV) scales, one must also consider SUGRA when dealing with inflation, and the no-scale SUGRA models [48] in particular are well suited for maintaining the flatness of the inflaton potential (thereby solving the η problem), although other approaches have also been discussed [49–53]. Also the Lyth bound [54] on the tensor-to-scalar ratio also suggests a scale of inflation below the Planck scale, leading

to testable at collider tests of inflation.

Ellis, Nanopoulos, Olive (ENO) have shown that no-scale SUGRA can behave like the successful Starobinsky inflationary model [55–57]. However, in the ENO approach, a term with constant modular weight is used to break SUSY, and there is no connection between inflation and SUSY breaking. Subsequently one of us has considered the above ENO model, but with a linear Polonyi term added to the superpotential [58]. The purpose of adding this term was to provide an explicit mechanism for breaking SUSY in order to provide a link between inflation and SUSY breaking. Indeed we showed that inflation requires a strict upper bound for the gravitino mass $m_{3/2} < 10^3$ TeV [58]. It was subsequently shown [59] how the model in [58] may be generalised to include the fields in the visible sector of the minimal supersymmetric standard model (MSSM). In such a framework the soft-SUSY breaking parameters depend on the modular weights in the superpotential and lead to new phenomenological possibilities for supersymmetry (SUSY) breaking, based on generalisations of no-scale SUSY breaking and pure gravity mediated SUSY breaking. The strict upper limit on the gravitino mass $m_{3/2} < 10^3$ TeV provides an important phenomenological constraint, bearing in mind that the gaugino masses are typically suppressed by a loop factor $1/(16\pi^2)$ in gravity mediated scenarios.

In the present paper, motivated by the desire to relate inflation to collider physics, including dark matter and the muon $g - 2$ measurement, we study the phenomenology of the no-scale SUGRA inflation model in [59]. Although related phenomenological studies of similar works have been undertaken [55–57] a full phenomenological study of the model in [59], which is subject to the upper bound on the gravitino mass, has not yet been undertaken. Here we shall perform a phenomenological study of two of the simplest cases suggested in [59]: the first case consisting of no-scale SUGRA with zero soft scalar masses $m_0 = 0$ and zero trilinear soft parameter $A_0 = 0$, where the only source of SUSY breaking in the visible sector is via the gaugino masses M_i ; the second case switches on a small soft trilinear mass $A_0 \neq 0$, while maintaining zero soft scalar masses $m_0 = 0$. In both cases we assume that the gaugino masses M_i (which are not fixed by the Kahler potential and are therefore independent of the details of inflation) to arise from a hybrid of anomaly mediated and universal sources [60]. Such gaugino masses M_i at the high scale will act as the seed of all soft squark and slepton masses at low energy via renormalisation group (RG) running effects. Given the small number of input parameters, we shall use a Monte Carlo scan over parameter space, using the SPheno [61, 62] package linked to FeynHiggs [63], MicrOmegas [64–68] and CheckMate [69, 70]. For each case above, we find viable regions of parameter space displaying the results in terms of a Likelihood function, including the requirement of successful dark matter relic density. We then consider a set of representa-

tive benchmark points from viable regions of parameter space, and discuss the prospects for discovering the resulting SUSY spectrum at colliders. In particular we show that the no-scale SUGRA case allows for dark matter while satisfying all phenomenological constraints, including the correct Higgs mass and dark matter relic density, leading to the prospect that SUSY may be discovered at the LHC or FCC.

The layout of the remainder of the paper is as follows. In section 2, we summarise the basic parameters of the no-scale SUGRA models that we analyse. In section 1 we describe our calculational approach and numerical tools and algorithms that we employ in the analysis. In section 4 we present our results for non-scale SUGRA case I, with all soft parameters equal to zero at the high scale apart from the gaugino masses. In section 5 we present our results for non-scale SUGRA case II, where we allow in addition (small) non-zero values of A_0 , which relaxes the collider constraints somewhat. Section 6 concludes the paper.

2 The no-scale SUGRA model parameters

In the considered model [59], the soft supersymmetry breaking parameters are well approximated by

$$\begin{aligned}
 m_0 &= 0 \\
 \frac{A_0}{m_{\frac{3}{2}}} &= -6\alpha, \\
 \frac{B_0}{m_{\frac{3}{2}}} &= 2(1 - \beta)
 \end{aligned}
 \tag{2}$$

where α, β are undetermined modular weights in the Kähler potential.

Turning to the gauginos, the model does not constrain the gaugino mass parameters. We therefore examine a general breaking scenario where the gaugino mass parameters are partly derived from "anomaly mediated" susy breaking giving three mass parameters. Each one is determined partly by loop corrections given below [71] and partly by a

universal term parameterised below by the dimensionless coefficient k [72],

$$\begin{aligned}
M_1 &= \left(\frac{33}{5} \frac{g_1^2}{16\pi^2} + k\right)m_{\frac{3}{2}}, \\
M_2 &= \left(\frac{g_2^2}{16\pi^2} + k\right)m_{\frac{3}{2}}, \\
M_3 &= \left(-3\frac{g_3^2}{16\pi^2} + k\right)m_{\frac{3}{2}}
\end{aligned}
\tag{3}$$

Note that the sign of k plays an important phenomenological role in determining the gaugino mass spectrum. For small and positive k the electroweak gaugino masses $M_{1,2}$ are enhanced while the magnitude of the gluino mass M_3 is reduced due to the partial cancellation against the negative anomaly mediated contribution. This yields a spectrum with a relatively light gluino and heavy winos and binos. On the other hand, for small and negative k , the electroweak gaugino masses $M_{1,2}$ are reduced due to a partial cancellation, while the magnitude of the gluino mass M_3 is increased. This yields a spectrum with relatively light winos and binos which is more suited to explaining the muon $g - 2$.

The supersymmetric theory produced by this model gives a very small set of high scale parameters; the scalar mass scale, m_0 , the bilinear coupling, B_0 , and the trilinear coupling, A_0 . In turn the two unified coupling parameters are determined by the gravitino scale $m_{\frac{3}{2}}$ and our choice of the modular weights α and β . Furthermore, m_0 is determined by our choice of Kähler potential [59]. In addition we choose a suitable value of $\tan(\beta)$ and μ to minimise the broken higgs potential and thus satisfy the higgs potential minimisation conditions given in [73]. We are therefore left with just five input parameters; α , β , $\tan(\beta)$, $m_{\frac{3}{2}}$ and μ , that must be selected in order to fully characterise the high scale model and its spontaneously broken characteristics. We shall mainly focus on the simplest cases $\alpha = 0$ and $\beta = 1$ which lead to zero soft parameters $A_0 = 0$ and $B_0 = 0$ at the high scale.

3 Method

The aim of this project is to Monte-Carlo scan over the small set of input parameters for the two cases given above. We do not use the Metropolis-Hastings algorithm [74]. This is simply because the input parameter set is so small that a random scan on the IRIDIS computer cluster will be suffice to cover the parameter landscape. We then calculate various experimental outcomes including collider phenomenology, mass spectrum, and dark matter relic density to calculate a likelihood associated with each parameter point.

We hope that this will give us a greater understanding of the model and its physical viability. We aim to place some lower bound on the gravitino mass scale thus constraining the model from above, via inflation constraints, and below, via Collider phenomenology. Furthermore, we hope to find some best fit parameter points that might satisfy the latest $g - 2$ results.

In order to understand the parameter space, we start with the simplest possible case, and subsequently increase its complexity. Therefore, initially we fix $\alpha = 0$ such that $A_0 = 0$. As B_0 is determined by electroweak symmetry breaking, we leave β and $\tan(\beta)$ as free parameters. SPheno also requires the $sign(\mu)$ to be prescribed. Although previous analyses suggest positive μ is more in-keeping with modern results, we chose to allow for both signs.

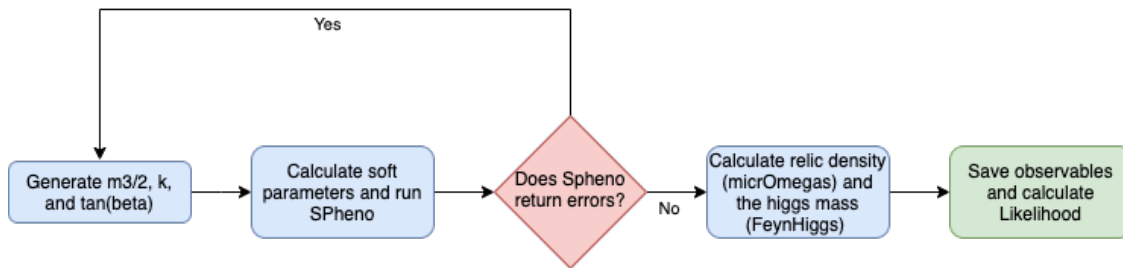


Figure 1: Shows the algorithm flow used for this analyses.

Generally speaking, the algorithm works as shown in Fig. 1. Four primary open source softwares were used to perform the calculations. For calculating the SUSY spectrum, $g - 2$, and a number of other , we chose to use a modified version of SPheno that printed the value of B_0 . Although for the most part our use of this software was very standard, we encountered a technical problem regarding the \overline{DR} renormalisation scheme. Large values of the gluino mass induce large logs that must be re-summed. To solve this we calculate the Higgs mass on-shell using FeynHiggs. In order to calculate the relic density, we use MicrOmegas.

For post data collection analysis we simulate collider effects using CheckMate [70]. This software combines a number of subsidiary packages to simulate the events in a collider and exclude any given model to a 95% confidence level. We chose to use $13TeV$ and $8TeV$ pp collision data with the ATLAS detector in a signal region that focused on the search for squarks and gluinos in final states with jets and missing transverse momentum

using $36fb$. This parameter space is commonly used in SUSY searches. However, further information could be garnered by broadening the analysis.

Instead of predefining β , as we did with α , and therefore fixing a value of B_0 , we decided to leave $\tan(\beta)$ as a free parameter to be scanned over. This affords us some flexibility in understanding the parameter space. Furthermore, with the results in hand it is simple to solve Equation 2 and find the relevant β parameter.

case	m_0	A_0	B_0	Section
I	0	0	$2(1 - \beta)m_{\frac{3}{2}}$	4
II	0	$-6\alpha m_{\frac{3}{2}}$	$2(1 - \beta)m_{\frac{3}{2}}$	5

Table 1: Table showing the two cases considered in this work. Gaugino mass terms (with a value for k), $\tan(\beta)$, the sign of μ , and the gravitino mass scale are also generated depending on the model being considered.

In order to fully explore the parameter space, a number of scans (and accordant parameter limits) were initialised. Each scan is assigned to a subsection and summarised in Table 2. Note that each scan is performed twice; once for $\mu > 0$ and again for $\mu < 0$.

	$m_{\frac{3}{2}}$ (TeV)	α	$\tan(\beta)$	k	Subsection
Scan 1	[1, 1000]	0	[1.5, 30]	[0, 0.1]	4.1
Scan 2	[1, 400]	0	[1.5, 50]	[-0.01, -0.04]	4.2
Scan 3	[1, 1000]	[-0.166, 0.166]	[1.5, 50]	[0, 0.1]	5.1
Scan 4	[1, 200]	[-0.005, 0.005]	[1.5, 50]	[-0.014, -0.035]	5.2

Table 2: Show the parameters for the 4 primary scans conducted in this paper. Links to the subsections in which each scan is presented are also included. In general, parameter ranges were chosen by trial an error so as to be representative of the parameter scape without losing excessive efficiency.

4 No-scale SUGRA with $A_0 = 0$ (Case I)

Completely no-scale SUGRA with $A_0 = 0$ represents a fascinating scheme for this model. Previously thought to be ruled out, such scale-less supersymmetry has seen something of a resurrection motivated by inflationary model building [75]. As shown in Table 1, $\alpha = 0$, and therefore $A_0 = 0$, precludes trilinear terms from the model. Although we

allow variance in β in order to understand the parameter space, we shall see a strong preference for $\beta \approx 1$ implying $B_0 = 0$ bilinear coupling too. With $m_0 = 0$ the scalar masses are all zero at the high scale, however, the gauginos get mass terms by Equation 3 and generate non-zero low energy scalar masses via the RGEs. Remarkably, it turns out that such a scheme is phenomenologically viable, as we shall see.

We begin by analysing the results of Scan 1 in Table 2, which assumes positive universal gaugino masses k , and allows the gravitino mass $m_{\frac{3}{2}}$ to vary up to its upper bound from inflation of 1000 TeV.

4.1 Positive k (Scan 1)

As discussed earlier, positive universal gaugino mass parameter k will tend to yield a spectrum with a relatively light gluino and relatively heavy winos and binos, so we do not expect this choice to explain the muon $g - 2$, so we will focus mainly on the Higgs mass and dark matter in this case. Figure 2 shows a scatter plot between the two most influential scan variables, k and $m_{\frac{3}{2}}$. It should be noted that, although $\tan(\beta)$ is a scan parameter, its influence on the overall likelihood is limited.

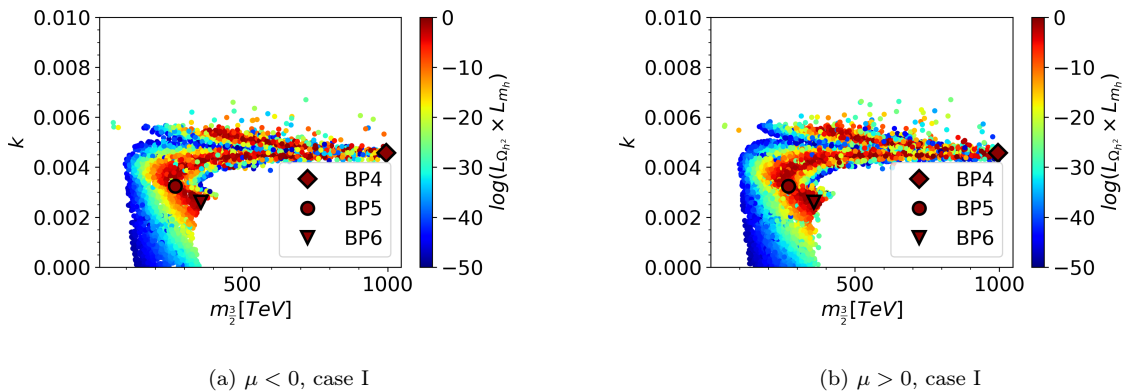


Figure 2: Shows k against $m_{\frac{3}{2}}$ for case I, $\alpha = 0$ data from a Monte-Carlo scan with parameter ranges $\tan(\beta) \in [1.5, 30]$, $k \in [0, 0.1]$, and $m_{\frac{3}{2}} \in [10^3 GeV, 10^6 GeV]$. Colour denotes likelihood, with hotter colours corresponding with high likelihoods. The likelihood is dominated by the relic density calculation. The range of k is naturally restricted to $k \lesssim 0.006$ due to $|\mu|^2 < 0$. Two bands of high likelihood points; one from above, one from below, converge at $(1000 TeV, 0.0044)$ in $(m_{\frac{3}{2}}, k)$ space. The 6 benchmarks that are presented in Table 3 are also marked. The central colour of the benchmark denotes its likelihood.

As points that failed to produce correct electroweak symmetry breaking or a suitable dark matter candidate have been excluded from these plots, a fascinating structure of allowed, disallowed, and high likelihood points emerges. Firstly, for values of $k \gtrsim 0.006$ electroweak symmetry breaking cannot be satisfied (except for some anomalous points that, due to numeric instability, achieve electroweak symmetry breaking). Secondly, for values of $k \lesssim 0.004$ with $m_{\frac{3}{2}} \gtrsim 400$ TeV the LSP becomes charged. This can be seen in Figure 3 where "cold" points tend to 0 mass difference and therefore, a charged LSP for large $m_{\frac{3}{2}}$ values.

In addition to the structure of excluded points, a band of hot points in the $(m_{3/2}, k)$ plane from (350 TeV, 0.0025) up to (250 TeV, 0.004) and across to (1000 TeV, 0.0045) where the relic density likelihood is maximised. An additional strip of high likelihood points begins at (400 TeV, 0.0055) and tracks down to (1000 TeV, 0.0046). We speculate that there could be some symmetry about $k \approx 0.0045$ that is broken above $k \approx 0.006$ due to electroweak symmetry breaking.

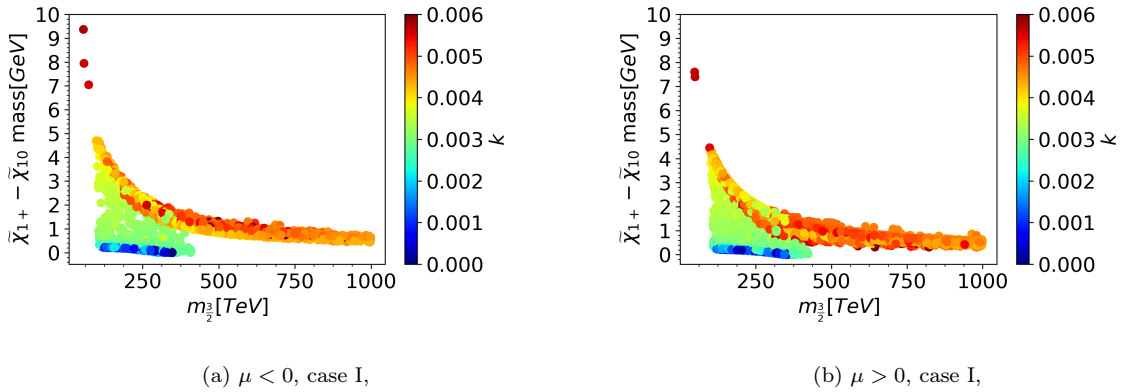


Figure 3: Shows the mass difference between the LSP and the nLSP for case I, $\alpha = 0$. The colour denotes the value of k . Small values of k lead to a negative difference between the $\tilde{\chi}_{1+}$ and $\tilde{\chi}_{10}$ at 400TeV implying a charged LSP.

The masses of the first two neutralinos are given by

$$\begin{aligned}
 m_{\tilde{\chi}_{10}} &= M_1 - \frac{m_W^2 (M_1 + \mu \sin(2\beta))}{\mu^2 - M_1^2} + \dots \\
 m_{\tilde{\chi}_{20}} &= M_2 - \frac{m_W^2 (M_2 + \mu \sin(2\beta))}{\mu^2 - M_2^2} + \dots
 \end{aligned}
 \tag{4}$$

And the first chargino by,

$$m_{\tilde{\chi}_{1+}} = M_2 - \frac{m_W^2(M_2 + \mu \sin(2\beta))}{\mu^2 - M_2^2} + \dots \quad (5)$$

From Table 5 we can see that as k reduces, the LSP becomes increasingly "wino-like". Therefore, the mass of the lightest neutralino is dominated by the mass of $m_{\tilde{\chi}_{20}}$ (Equation 4). In turn, the mass of lightest chargino is given, to leading order, by the same expression (Equation 5). Therefore, their masses are exceptionally close. Although this can be helpful in reducing the relic density by some co-annihilation processes, for high $m_{\frac{3}{2}}$ the contributing factors can lead to a switch in hierarchy between the two mass states. This is further confirmed in Figure 3 where the mass difference between the LSP and the nLSP tends to 0 for small k .

In this case $m_0 = 0$ and thus the susy scale is relatively low. Therefore, it is important to consider the spectrum masses, their potential collider signature, and the effect new SUSY diagrams could have on certain branching ratios. We begin by looking at the mass distributions of the SUSY spectrum.

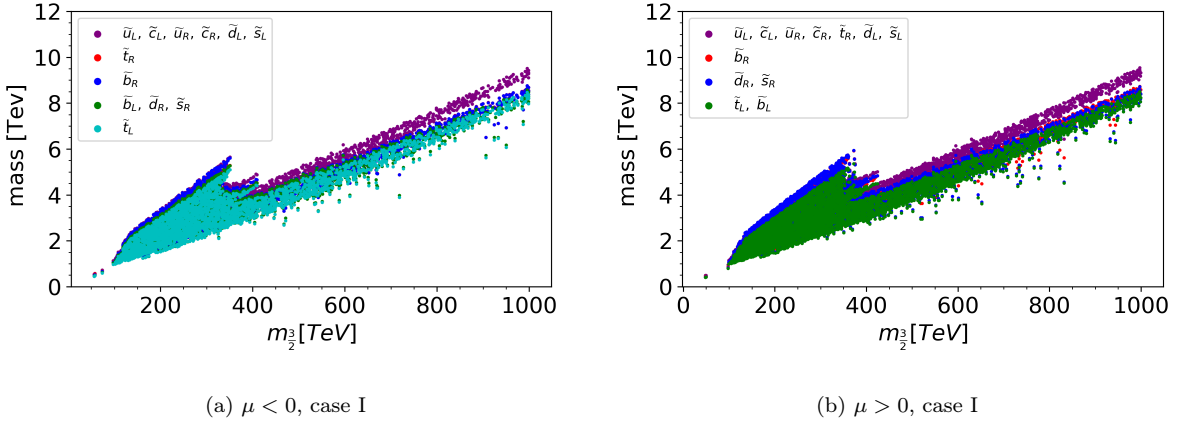


Figure 4: Shows the squark mass spectrum for case I, $\alpha = 0$. Particles are plotted in the same colour if they are sufficiently mass degenerate as to be indistinguishable in this plot. Typically, this would entail masses within 15GeV of each other. Increasing k increases the mass of the squarks. Low k points cut-off just below $400TeV$.

From Fig 4, we see the mass distribution of the squarks with respect to $m_{\frac{3}{2}}$. Although it is not explicitly plotted we can see the effect of k variance as a part of the mass distribution seems to cut-off just below $400TeV$. This is a reflection of the point demonstrated in

Figure 3, where low k points tend to having a charged LSP for large $m_{\frac{3}{2}}$. This same dependence of k can also be seen in Figures 5 and 6.

We see that a reduction in k increases the overall scale of the squarks. Their mass is given predominantly by M_3 contributions. Therefore, a reduction of k will lead to an increase in the absolute value of M_3 as, by Equation 3, the anomaly mediated term is negative. This increase in mass scale leads to an increase in the mass scale of the squarks. We also note that the left handed \tilde{t} tends to be the the lightest squark with the first generation squarks making up the heaviest squarks as is typical in such models without flavour mixing.

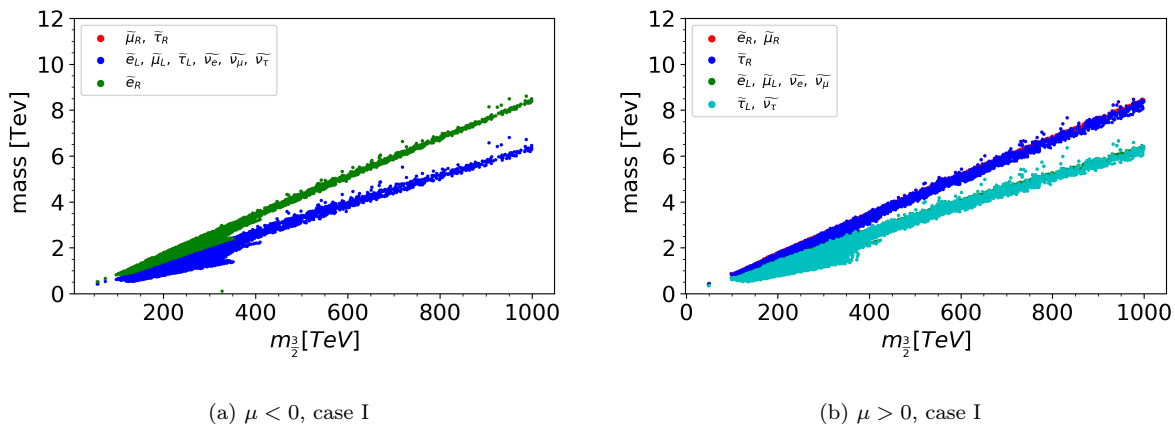


Figure 5: As in Figure 4 but showing the slepton masses. Increasing k decreases the mass of the sleptons. Low k points cut-off just below 400TeV .

Unlike the squarks, a reduction in k decreases the mass scale of the sleptons. As they are uncharged under $SU(3)$, they receive their mass from contribution from M_1 and M_2 . Furthermore, their anomaly mediated terms are positive, so a reduction in k leads to a reduction in their absolute scale and thus a reduction in the slepton masses. Analogously to the squarks, the left handed $\tilde{\tau}$ states tend to be the lightest sleptons.

Perhaps predictably, given the scaleless nature of the model, Figure 6 shows the most interesting structure with regard to the mass spectrum. Firstly, as $m_{\frac{3}{2}}$ increases, the hierarchy of the heaviest neutralino and the gluino reverse. Furthermore, as k increases, the gluino mass increases significantly. This can be understood by a similar argument to that of the squarks; an increase in k leads to a decrease in the absolute scale of M_3 and thus a decrease in the gluino mass.

Furthermore, for large values of k the first neutralino mass, χ_{10} , does not depend on $m_{\frac{3}{2}}$.

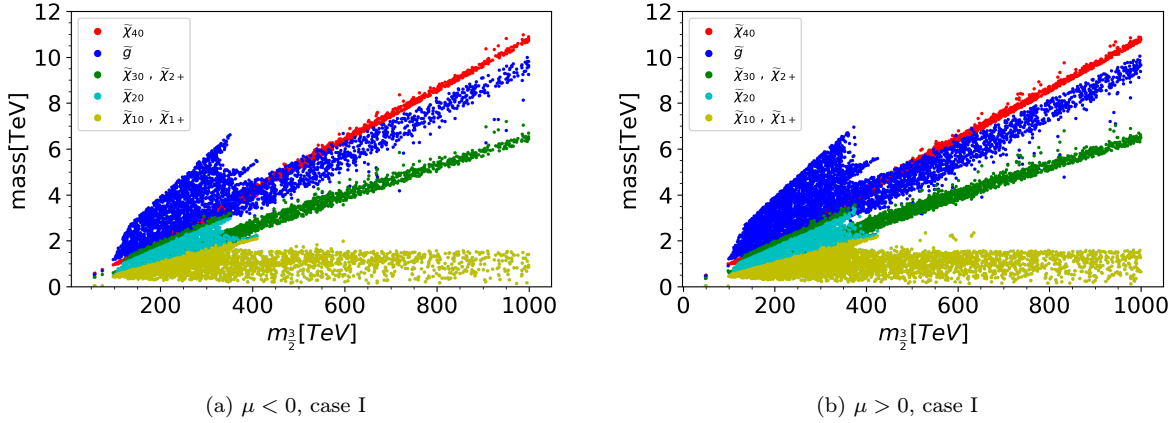


Figure 6: As in Figure 4 but showing the gaugino masses. Increasing k decreases the mass of the gauginos. Low k points cut-off just below 400TeV .

The large values of k increase the proportion of the first neutralino that is "higgsino-like". As this mass depends predominantly on μ , this stabilises the mass of the neutralino with respect to $m_{\frac{3}{2}}$. Conversely, small k creates a "wino-like" neutralino whose mass is proportional to M_2 and thus to $m_{\frac{3}{2}}$.

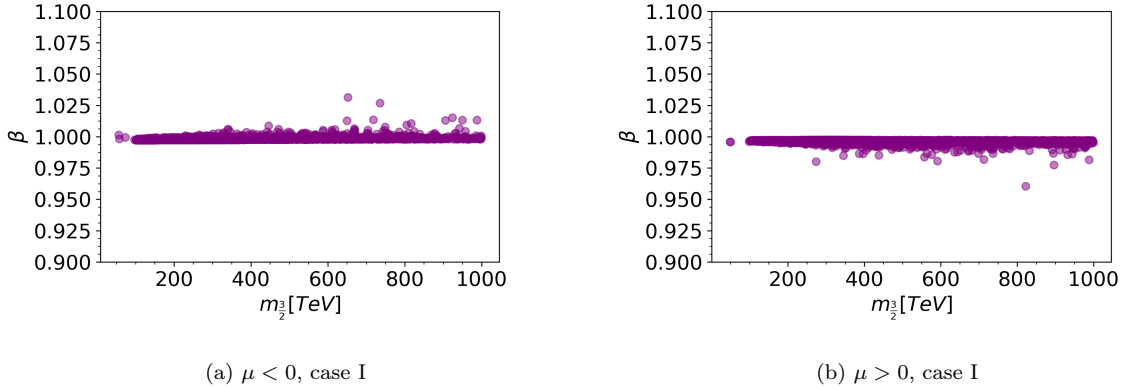


Figure 7: Shows the values of the modular weight, β , produced for case I, $\alpha = 0$. There is a natural tendency for values very close to 1. According to Eq. 2, this suggests $B_0 \approx 0$, in-keeping with scale-less supersymmetry or no-scale SUGRA.

Due to the different natures of the model weights, we decided to allow $\tan(\beta)$, and therefore B_0 and β^3 , to vary as a free parameter but keep α fixed. Therefore, it is interesting

³ β is used both as the inverse tangent of the ratio of the higgs vevs, and as the modular weight. From

to see the implications of the scan for the free β parameter. Looking at Fig 7 we find a striking prediction for the model. For both signs of μ this model predicts that $\beta \approx 0.998$ (excluding some anomalous points). Recall that, by Eq. 2, β is connected to the bilinear coupling such that if $\beta = 1 \implies B_0 = 0$. As can be seen, the model clearly favours a bilinear coupling very close to 0 making a fully scale-less model.

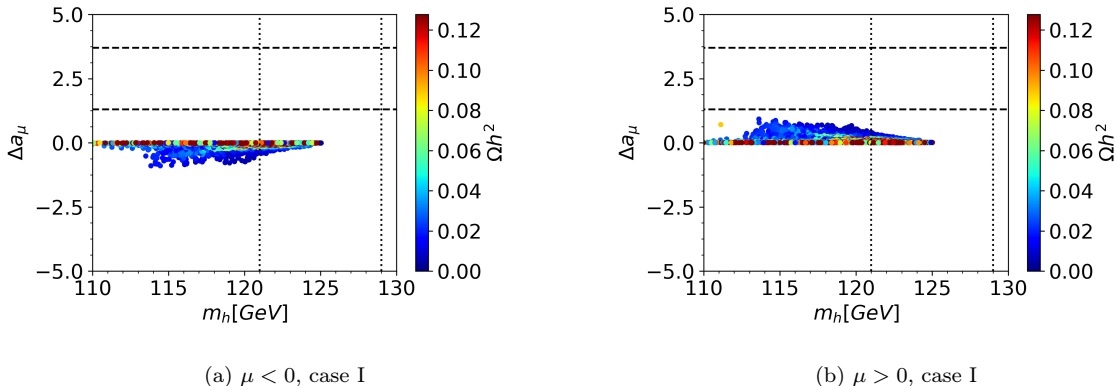


Figure 8: Shows a scatter plot of the higgs mass against the anomalous muon magnetic moment for a scan with ranges $\tan(\beta) \in [1.5, 30]$, $k \in [0, 0.1]$, and $m_{\frac{3}{2}} \in [10^3 GeV, 10^6 GeV]$. The 2σ region of a_μ is marked with dotted lines while the 2σ region of m_h is marked with dashed lines. The colour denotes the relic density. No point satisfies the observed values of the muon $g - 2$.

From Figure 8 we see that this model cannot satisfy this condition for either sign of μ . In the $\mu < 0$ case, we see that the contributions are in fact negative. The contributions generally take the form $\Delta a_\mu \propto \text{sign}[\mu] \frac{1}{(m_{\tilde{\mu}, \tilde{\nu}_\mu})^2}$. Therefore, a change in the sign of μ reverses the sign of these contributions. In general, large $m_{\frac{3}{2}}$ leads to a large mass spectrum which in turn suppresses the $g - 2$ contributions. From Figure 5 we can see that the masses of the $\tilde{\mu}s$ and $\tilde{\nu}_\mu s$ grow linearly with $m_{\frac{3}{2}}$ leading to quadratic suppression of Δa_μ . Although in the positive μ case, the contributions are themselves positive, no point can satisfy the measured discrepancy.

To gain further insight into this model, a set of benchmark points is presented. Table 3 shows the input parameters for each benchmark point selected. The benchmark points were selected to reflect a variety of viable regions in the model.

Benchmark points 1,2, and 3 all have their sign of μ positive while the reverse is true for points 4,5, and 6. BP1 and BP4 are the highest likelihood points of the model for their respective signs of μ . BP4 comes from the second band of high likelihood points at context it should be clear which is being referred to.

Quantity	BP1	BP2	BP3	BP4	BP5	BP6
α	0	0	0	0	0	0
β	0.996	0.997	0.997	0.998	0.998	0.998
$m_{\frac{3}{2}}$ [TeV]	903	268	359	995	269	358T
k	0.00443	0.00323	0.00251	0.00457	0.00324	0.0026
<u>SPheno:</u>						
m_0 [GeV]	0	0	0	0	0	0
$\tan(\beta)$	18.1	23.9	19.6	29.3	20.0	29.6
$\text{sign}(\mu)$	1	1	1	-1	-1	-1
A_0 [GeV]	0	0	0	0	0	0
M_1 [GeV]	20800	5700	7600	23000	5900	7600
M_2 [GeV]	6800	1700	2000	7600	1700	2000
M_3 [GeV]	-4400	-1600	-2400	-4700	-1600	-2400

Table 3: Shows six benchmark points representing six different areas of interest in the parameter where case I, $\alpha = 0$. We present the model parameters and the resultant SPheno input parameters. BP1 and BP4 show the highest likelihood points for $\mu > 0$ and $\mu < 0$ respectively. BP2 and BP5 show points where $m_{\frac{3}{2}}$ is minimised whilst still satisfying our main constraints for $\mu > 0$ and $\mu < 0$ respectively. BP3 and BP6 show points for minimal values of k whilst still satisfying our main constraints for $\mu > 0$ and $\mu < 0$ respectively. Dimensions of the parameters are given where "-" means dimensionless. $m_{\frac{3}{2}}$ is given in units of TeV, and m_0, A_0, M_i are given in GeV.

$k > 0.0045$. They both have very high $m_{\frac{3}{2}}$ values existing just below the cut-off set by the CMB in the context of inflation [59]. BP2 and BP5 have the lowest values of $m_{\frac{3}{2}}$ whilst staying in a high likelihood range and BP3 and BP6 have the lowest values of k whilst staying in a high likelihood range.

Table 4 shows the resultant SUSY mass spectrum for the 6 benchmark points presented so far. As changing the sign of μ plays little role, we will refer to the combination of BP1 and BP4 as BP14, and similarly for the other benchmark points. Many points do not achieve a the precise value for the higgs mass. However, there is a relatively large theoretical uncertainty on this parameter leaving all these points with relatively high likelihoods.

BP14 shows a hugely inflated mass spectrum for the squarks and sleptons. Furthermore, we see huge masses for the heaviest gauginos. However, although much of the spectrum is high in mass, the lighter gauginos are only about 1TeV. These could leave a tell tale signature in current or future colliders. We also see a relatively low μ value. This causes the high "higgsino-like" proportions of the LSP. $\tilde{\nu}_{\tau L}$ is the smallest supersymmetric scalar

Masses	BP1	BP2	BP3	BP4	BP5	BP6
\tilde{e}_L	5690	1540	1900	6340	1540	1910
\tilde{e}_R	7590	2160	2790	8400	2170	2790
$\tilde{\nu}_{eL}$	5690	1530	1890	6340	1540	1910
$\tilde{\mu}_L$	5690	1540	1900	6340	1540	1910
$\tilde{\mu}_R$	7590	2160	2790	8400	2170	2790
$\tilde{\nu}_{\mu L}$	5690	1530	1890	6330	1540	1910
$\tilde{\tau}_1$	5690	1490	1860	6100	1510	1820
$\tilde{\tau}_2$	7460	2100	2740	8040	2130	2680
$\tilde{\nu}_{\tau L}$	5610	1490	1860	6100	1510	1820
\tilde{d}_L	8580	3190	4500	9260	3190	4450
\tilde{d}_R	7780	3060	4390	8310	3060	4330
\tilde{u}_L	8580	3190	4500	9260	3190	4450
\tilde{u}_R	8920	3300	4680	9620	3310	4630
\tilde{s}_L	8580	3190	4500	9260	3190	4450
\tilde{s}_R	7780	3060	4390	8310	3060	4330
\tilde{c}_L	8580	3190	4500	9260	3190	4450
\tilde{c}_R	8920	3300	4680	9620	3310	4630
\tilde{b}_1	7670	2910	4160	8040	2940	4090
\tilde{b}_2	7870	2980	4320	8420	3020	4230
\tilde{t}_1	7600	2840	4050	8190	2840	4010
\tilde{t}_2	7880	2940	4170	8420	2960	4110
\tilde{g}	8940	3510	5080	9540	3510	5010
$\tilde{\chi}_{10}$	1110	1370	1750	1110	1370	1770
$\tilde{\chi}_{20}$	1111	1410	2170	1110	1400	2110
$\tilde{\chi}_{30}$	5810	1500	2170	6520	1500	2110
$\tilde{\chi}_{40}$	9650	2620	3440	10800	2640	3440
$\tilde{\chi}_{1+}$	1110	1370	1750	1110	1370	1770
$\tilde{\chi}_{2+}$	5810	1500	2180	6520	1500	2110
h_0	124.5	120	122	125	121	123
H_0	5510	1860	2690	5410	1970	2520
A_0	5510	1860	2690	5410	1970	2520
H_{\pm}	5520	1870	2700	5410	1970	2520
μ	1100	1400	2100	-1070	-1390	-2090
B_0	7610	1510	1970	3890	1240	1700

Table 4: Shows the spectrum of SUSY masses for the benchmark points given in Table 3. The difference between the mass of $\tilde{\chi}_{1+}$ and $\tilde{\chi}_{10}$ is also given as this pertains to the production of dark matter. We also include the highscale bilinear coupling value B_0 for its relevance to the high scale parameters of the model. All masses are given in GeV.

Quantity	BP1	BP2	BP3	BP4	BP5	BP6
$\Omega_{DM}h^2$	0.119	0.124	0.115	0.119	0.119	0.124
$\tilde{\chi}_{10}$ [GeV]	1109.5	1372.7	1748.3	1110.5	1372.1	1767.0
$\tilde{\chi}_{1+} - \tilde{\chi}_{10}$ [GeV]	0.48072	1.5	0.0329	0.59656	1.699	0.03567
$ \alpha_1 ^2$	0.000016	0.000441	0.000004	0.000009	0.0004	0.000004
$ \alpha_2 ^2$	0.000144	0.312481	0.982081	0.0001	0.228484	0.976144
$ \alpha_3 ^2$	0.499849	0.352836	0.011025	0.499849	0.394384	0.014161
$ \alpha_4 ^2$	0.499849	0.335241	0.007396	0.499849	0.375769	0.009604

Table 5: Shows the relic density of the LSP for each benchmark point. The difference between the LSP and the nLSP is also given. Finally, we give the probability of finding the given LSP in a particular flavour state. That is to say; we give $|\alpha_i|^2$ where $\tilde{\chi}_{10} = \alpha_1\tilde{B} + \alpha_2\tilde{W} + \alpha_3\tilde{H}_1 + \alpha_4\tilde{H}_2$ and $\sum |\alpha_i|^2 = 1$. Dimensionful parameters are given in GeV.

(excluding the higgs boson).

BP25 shows a significantly reduced SUSY spectrum due to the reduced scale of $m_{\frac{3}{2}}$ and therefore the reduction in $M_{1,2,3}$. Although the majority of the spectrum is still mostly out of range of modern detectors, the model still produces low mass light gauginos. Although the mass gap between $\tilde{\chi}_{10}$ and $\tilde{\chi}_{1+}$ is still small, the gap between the first two charged states has increased due to a change in the mixing of the gauginos. Again, $\tilde{\nu}_{\tau L}$ is the smallest supersymmetric scalar.

Finally, BP36 shows a slight increase in the overall SUSY scale in comparison to the BP25. Although the mass gap between the heavy and light gaugino states has increased, the overall scale for the states has increased significantly as the LSP becomes almost exclusively "wino-like". In general, a high wino-like state can lead to excessive co-annihilation with the first chargino; especially when, as can be seen in Table 5, the mass gap between said states is so low. However, for sufficiently high mass neutralinos, the freeze out temperature is high thus ending these problematic processes early in the universes cosmological past and thereby preventing the excessive annihilation of the candidate. Although $\tilde{\chi}_{1+}$ is still the second lowest mass particle, the $\tilde{\nu}_{\tau L}$ is lighter than the $\tilde{\chi}_{20}$ unlike in the other benchmark points where a clear hierarchy existed between the fermionic and scalar states.

Table 5 shows information specifically regarding the relic density for the benchmarks points. In all cases we see a very compressed gaugino mass spectrum inducing the requisite co-annihilation processes. BP36 shows an exceptionally compressed mass gap. As was previously argued, the high mass leads to an early freeze out temperature preventing these co-annihilation processes eradicating the dark matter too efficiently. We also present the

proportion of bino, wino, and higgsino for the given particle. We see a very interesting shift between the respective benchmark points with BP14 being mostly higgsino, BP25 being evenly split between higgsino and wino, and BP36 being majority wino.

Tables 6, 7, 8 show phenomenological information regarding potential constraints and collider physics. BP1 and BP4, BP2 and BP5, and BP3 and BP6 are paired together as they belong to similar regions of parameter space. We implemented a checkmate analysis for both 8, 13, and 14 TeV ATLAS and CMS analyses. However, we chose not to include 14TeV analysis in our tables as they are not based on LHC runs but rather Monte-Carlo simulations. Instead, where appropriate, we have simply noted the r_{max} value (defined below) produced as suggestive of the type of the effects future colliders could have. We use MadGraph_2.6.7 [76,77] to generate events with SUSY final states. Pythia_8.2.45 [78,79] is then used to shower and hadronise the events. Finally, Delphes_3.4.2 [80] and some subsidiary tools [81–84] are used to perform event and detector analysis. This approach allows us to assess a given benchmark points viability in comparison with experimental data. We find that all presented benchmark points cannot be ruled out by the LHC at $\sqrt{s} \leq 13TeV$. We include a quantity r_{max} defined by

$$r_{max} = \frac{S - 1.64 \cdot \Delta S}{S95} \quad (6)$$

where S is the number of signal events, ΔS is its uncertainty, and $S95$ is the experimental upper limit on the number of signal events. This quantity indicates whether a point is ruled out by the analyses or not. Points with $r_{max} \geq 1$ are ruled out; those with $r_{max} < 1$ are not. We also include the total proton to proton collision cross section, σ_{LO} at the given centre of mass energy. Finally, the most important signal regions analysed by CheckMATE are given. We find a variety of different analyses are important due to the changing mixing matrices and SUSY spectrum.

We include a number important beyond the standard model constraints; Δa_μ , BR ($B_s \rightarrow \mu^+ \mu^-$), the relic density, and BR ($b \rightarrow s \gamma$). We find that the two branching ratios agree with experimental data very well. However, the lack of light $\tilde{\mu}s$ and $\tilde{\nu}_\mu s$ lead to insufficient contributions to the Δa_μ loop diagrams as these are suppressed by the propagator mass squared. Indeed, BP4, 5, and 6 have negative contributions to the anomalous muon magnetic moment. This is due to the reversal of sign of the μ parameter, and the dependency on μ in the gaugino mediated diagrams that contribute to Δa_μ . As the relic density is our strongest constraint, all points have been chosen to satisfy modern cosmological constraints on the production of dark matter.

Finally, we include the decay width and branching ratios of the two lightest particles (excluding the LSP who is stable). In BP14 and BP25 these are light gaugino states. However, in BP36, the $\tilde{\nu}_\tau$ is lighter than the χ_{20} . Only branching ratios that contribute by more than 1% are included.

Although BP14 shows a long lifetime it is drastically insufficient for the particle to escape the detector. Therefore, the particles decay products are very important in assessing the signature of this model. The analysis region of most significance is one that focuses on mono-jets. This analysis has a very large luminosity. It should be noted that, unlike BP25 and BP36, 14TeV analysis yields an r_{max} value of 0, perhaps due to the lack of significance at such high energy scales. The branching ratios for both the two lightest non-LSP particles are dominated by $\tilde{\chi}_{10}$ decays. This would suggest large corresponding missing momenta. We find an excellent fit for the BSM constraints as well as dark matter. However, Δa_μ cannot be satisfied.

The most constraining region for BP25 focuses on squarks and gluinos, with 0 leptons, and 2-6 jets at 13TeV. This is due to the relatively low mass of the strongly coupled particles. We see the highest value of r_{max} of all the benchmark points due to the abundance of these lighter particles. $\tilde{\chi}_{20}$ shows a huge variety in decay channels as the mass gap is too small for the squark pairs to hadronise. We find that 14TeV analysis yields very high r_{max} values of 0.276 in the positive μ case. This suggests that future colliders could probe regions of interest in this model. Again, the relic and BSM branching ratios can be fitted well, but Δa_μ cannot.

As previously eluded to, BP36 shows a change in the spectrum hierarchy. From Table 5, the mass difference between $\tilde{\chi}_{10}$ and $\tilde{\chi}_{1+}$ is the smallest. Therefore, a smaller phase space is available leading to fewer decay channels. In contrast to $\tilde{\nu}_\tau$, whose lifetime is very small, the lifetime of χ_{1+} is sufficiently long that the particle could escape the detector. As it is a charged particle, this would appear as a charge track in the calorimeter. As was the case for BP25, 14TeV analysis gives a whole order of magnitude increase in r_{max} hinting at the exciting prospects for physics to come. Again, the BSM constraints and the relic are satisfied; however, Δa_μ is not.

Quantity	BP1	BP4
$\Gamma_{\chi_{1+}}$ [GeV]	8.4×10^{-14}	1.7×10^{-13}
BR ($\chi_{1+} \rightarrow \chi_{10} \pi^+$) [%]	92.9	89.3
BR ($\chi_{1+} \rightarrow \chi_{10} e^+ \nu_e$) [%]	4.00	5.71
BR ($\chi_{1+} \rightarrow \chi_{10} \mu^+ \nu_\mu$) [%]	3.14	4.90
$\Gamma_{\chi_{20}}$ [GeV]	5.12×10^{-12}	2.9×10^{-12}
BR ($\chi_{20} \rightarrow \chi_{10} \pi^0$) [%]	63.8	74
BR ($\chi_{20} \rightarrow \chi_{1+} \pi^-$) [%]	6.1	2.64
BR ($\chi_{20} \rightarrow \chi_{1-} \pi^+$) [%]	6.1	2.64
BR ($\chi_{20} \rightarrow \chi_{10} \gamma$) [%]	4.9	5.79
BR ($\chi_{20} \rightarrow \chi_{10} e^- e^+$) [%]	2.0	1.81
BR ($\chi_{20} \rightarrow \chi_{10} \mu^- \mu^+$) [%]	2.0	1.72
BR ($\chi_{20} \rightarrow \chi_{10} \nu_e \bar{\nu}_e$) [%]	2.0	10.8
BR ($b \rightarrow s \gamma$) [%]	0.032	0.032
BR ($B_s \rightarrow \mu^+ \mu^-$) [%]	2.9×10^{-7}	2.9×10^{-7}
Δa_μ	8.39×10^{-12}	-1.15×10^{-11}
$\Omega_{DM} h^2$	0.119	0.119
χ_{10} [GeV]	1110	1110
$\sigma_{q\bar{q} \rightarrow \chi_{10} \chi_{10}}$ [pb]	0	0
r_{max}	3.72×10^{-4}	2.03×10^{-4}
\sqrt{s} [TeV]	13	13
Analysis	atlas_conf_2017_060	atlas_conf_2017_060
Signal Region	EM7	IM6
Ref.	[85]	[85]
σ_{LO} [pb]	4.126×10^{-4}	4.036×10^{-4}

Table 6: Shows branching ratios for lightest supersymmetric particles in the spectrum for the benchmark points with highest likelihood, BP1 and BP4. Only branching ratios greater than 1% are included. We also include some of the beyond the standard model observables BR ($b \rightarrow s \gamma$), BR ($B_s \rightarrow \mu^+ \mu^-$), Δa_μ , and $\Omega_{DM} h^2$, where Δa_μ is a calculation of the SUSY contribution beyond the standard model. The model successfully predicts the b decays discrepancy as well as the relic density. However, the anomalous muon magnetic moment cannot be satisfied. CheckMATE runs using 13TeV and 8TeV analyses cannot rule out these points. The cross section σ_{LO} is calculated by pythia as a summation of subprocesses giving the total p+ p+ cross section. Decay widths and masses are given in GeV, branching ratios are given in %, and cross sections are given in pb.

Quantity	BP2	BP5
$\Gamma_{\chi_{1+}}$ [GeV]	8.9×10^{-12}	1.4×10^{-11}
BR ($\chi_{1+} \rightarrow \chi_{10} \bar{d} u$) [%]	60.0	58.9
BR ($\chi_{1+} \rightarrow \chi_{10} \bar{s} c$) [%]	0.34	2.02
BR ($\chi_{1+} \rightarrow \chi_{10} e^+ \nu_e$) [%]	20.1	19.7
BR ($\chi_{1+} \rightarrow \chi_{10} \mu^+ \nu_\mu$) [%]	19.6	19.4
$\Gamma_{\chi_{20}}$ [GeV]	2.45×10^{-4}	6.1×10^{-5}
BR ($\chi_{20} \rightarrow \chi_{10} u \bar{u}$) [%]	3.92	4.22
BR ($\chi_{20} \rightarrow \chi_{10} c \bar{c}$) [%]	3.90	4.18
BR ($\chi_{20} \rightarrow \chi_{10} d \bar{d}$) [%]	5.09	5.49
BR ($\chi_{20} \rightarrow \chi_{10} s \bar{s}$) [%]	5.09	5.49
BR ($\chi_{20} \rightarrow \chi_{10} b \bar{b}$) [%]	4.68	4.74
BR ($\chi_{20} \rightarrow \chi_{10} e^- e^+$) [%]	1.17	1.26
BR ($\chi_{20} \rightarrow \chi_{10} \mu^- \mu^+$) [%]	1.17	1.26
BR ($\chi_{20} \rightarrow \chi_{10} \tau^- \tau^+$) [%]	1.16	1.24
BR ($\chi_{20} \rightarrow \chi_{10} \nu_e \bar{\nu}_e$) [%]	7.03	7.57
BR ($\chi_{20} \rightarrow \chi_{1+} d \bar{u}$) [%]	11.2	10.8
BR ($\chi_{20} \rightarrow \chi_{1-} \bar{d} u$) [%]	11.2	10.8
BR ($\chi_{20} \rightarrow \chi_{1+} s \bar{c}$) [%]	11.1	10.7
BR ($\chi_{20} \rightarrow \chi_{1-} \bar{s} c$) [%]	11.1	10.7
BR ($\chi_{20} \rightarrow \chi_{1+} e^- \bar{\nu}_e$) [%]	3.72	3.60
BR ($\chi_{20} \rightarrow \chi_{1-} e^+ \nu_e$) [%]	3.72	3.60
BR ($\chi_{20} \rightarrow \chi_{1+} \mu^- \bar{\nu}_\mu$) [%]	3.72	3.60
BR ($\chi_{20} \rightarrow \chi_{1-} \mu^+ \nu_\mu$) [%]	3.72	3.60
BR ($\chi_{20} \rightarrow \chi_{1+} \tau^- \bar{\nu}_\tau$) [%]	3.68	3.54
BR ($\chi_{20} \rightarrow \chi_{1-} \tau^+ \nu_\tau$) [%]	3.68	3.54
BR ($b \rightarrow s \gamma$) [%]	0.033	0.033
BR ($B_s \rightarrow \mu^+ \mu^-$) [%]	2.9×10^{-7}	3.0×10^{-7}
Δa_μ	1.15×10^{-10}	-9.6×10^{-11}
$\Omega_{DM} h^2$	0.124	0.119
χ_{10} [GeV]	1370	1370
$\sigma_{q\bar{q} \rightarrow \chi_{10} \chi_{10}}$ [pb]	8.629×10^{-8}	2.718×10^{-8}
r_{max}	1.12×10^{-2}	8.10×10^{-3}
\sqrt{s} [TeV]	13TeV	13TeV
Analysis	atlas_1712_02332	atlas_1712_02332
Signal Region	2j-3600	2j-3600
Ref.	[86]	[86]
σ_{LO} [pb]	1.611×10^{-4}	1.630×10^{-4}

Table 7: As in Table 6 but for BP2 and BP5; points with low $m_{\frac{3}{2}}$.

Quantity	BP3	BP6
$\Gamma_{\chi_{1+}}$ [GeV]	7.2×10^{-20}	1.0×10^{-19}
BR ($\chi_{1+} \rightarrow \chi_{10} \bar{d} u$) [%]	72	72
BR ($\chi_{1+} \rightarrow \chi_{10} e^+ \nu_e$) [%]	28	28
$\Gamma_{\tilde{\nu}_\tau}$ [GeV]	2.9×10^{-1}	7.7×10^{-2}
BR ($\tilde{\nu}_\tau \rightarrow \chi_{10} \nu_\tau$) [%]	33.3	33.0
BR ($\tilde{\nu}_\tau \rightarrow \chi_{1+} \tau^-$) [%]	66.7	67.0
BR ($b \rightarrow s \gamma$) [%]	0.032	0.032
BR ($B_s \rightarrow \mu^+ \mu^-$) [%]	2.9×10^{-7}	3.0×10^{-7}
Δa_μ	5.50×10^{-11}	-8.30×10^{-11}
$\Omega_{DM} h^2$	0.115	0.124
χ_{10} [GeV]	1750	1750
$\sigma_{q\bar{q} \rightarrow \chi_{10} \chi_{10}}$ [pb]	7.805×10^{-8}	6.467×10^{-8}
r_{max}	3.458×10^{-3}	3.189×10^{-3}
\sqrt{s} [TeV]	13TeV	13TeV
Analysis	atlas_conf_2017_060	atlas_conf_2017_060
Signal Region	EM10	EM10
Ref.	[85]	[85]
σ_{LO} [pb]	1.520×10^{-5}	1.422×10^{-5}

Table 8: As in Table 6 but for BP3 and BP6; points with low k .

4.2 Negative k (Scan 2)

In this case we expect a negative universal gaugino mass parameter k to tend to yield a spectrum with a heavy gluino and relatively light winos and binos, possibly suitable to explain the muon $g - 2$, as well as the Higgs mass and dark matter. Moreover, in order to explain the measured Δa_μ , small values of the $\tilde{\mu}$ mass are required. As seen in Figures 4, 5, and 6, a reduction in k reduces the slepton masses, whilst increasing the gluon and squark masses. Further reductions in k reduce the $\tilde{\mu}$ mass sufficiently but keep the mass of the higgs boson high as this is dependant on the SU(3) charged squarks and sleptons.

In Scan 2, the k parameter is varied from 0 to -0.04 . As noted, negative values of k will increase the absolute scale of M_3 but reduce the scale of M_2 . This will further contribute to the effect described above, increasing squark masses whilst decreasing slepton masses. As previously argued, the Δa_μ contributions depend on $m_{\tilde{\mu}}^{-2}$ and therefore large values of $m_{\frac{3}{2}}$ will lead to a suppression of the contributions. We therefore scan for lower values of $m_{\frac{3}{2}}$ between 0 and 400 TeV.

Fig 9 shows the distribution of k against $m_{\frac{3}{2}}$ for both signs of μ . As we are now focussing on a_μ we redefine the likelihood as $L = L_{a_\mu} \times L_{m_h}$. However, we do not want relic particles whose abundance would rule out the model entirely. Therefore, we impose the condition that $\Omega h^2 < 0.12 + 2 \times 0.0078$ such that no point can be ruled out by leaving a non-phenomenologically large relic abundance.

From Fig 9, we see two distinct areas of points that give viable results; $k \approx -0.016$ and $k \approx -0.023$. However we find that $k \approx -0.023$ with $\mu < 0$ is phenomenologically preferred. In this region, we also find $30\text{TeV} < m_{\frac{3}{2}} < 100\text{TeV}$ to be preferred.

Finally, we present the results of a scan focussing on the good region as seen in Figure 10 where k varies between -0.022 and -0.027 and the sign of μ is fixed as negative. Negative results for Δa_μ are now ruled out as the absolute value of the gaugino mass parameters is large, suppressing some key SUSY contributions to $(g - 2)$ that involve these particles. This leaves us with one first order loop diagram that contributes to this result whose sign is fixed by the sign of μ .

Figure 10 shows the distribution of Δa_μ against the higgs mass. We see many points sit within the 2σ region. Furthermore, we find that many of these points have excellent dark matter relic densities. Two benchmark points are marked on Figure 10 who are presented later.

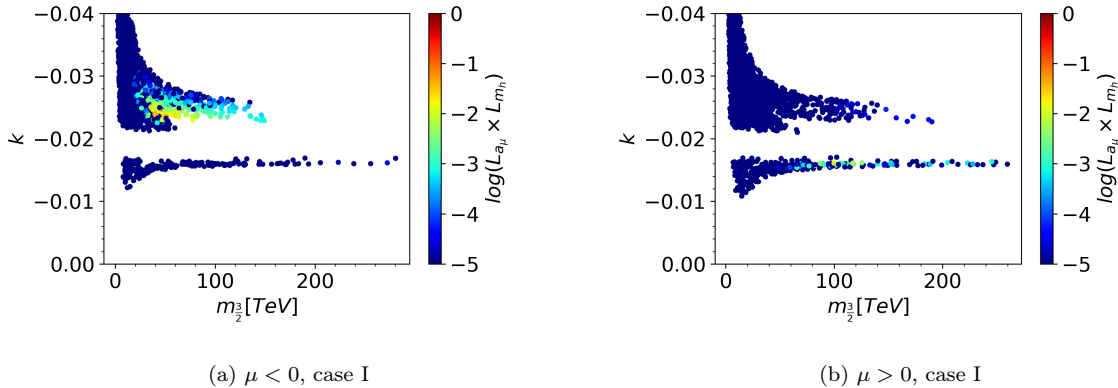


Figure 9: Shows the distribution of k against $m_{3/2}$ with a_μ and m_h log likelihood for $m_{3/2} \in [0\text{TeV}, 400\text{TeV}]$, $\alpha = 0$ and $k \in [-0.035, -0.014]$. A region with $\mu < 0$, $k \approx -0.023$ and $m_{3/2} \in [40\text{TeV}, 60\text{TeV}]$ is preferred.

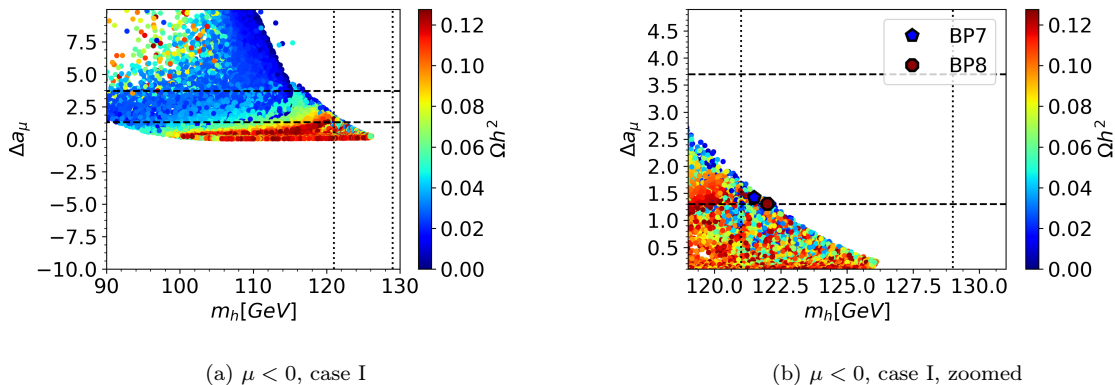


Figure 10: Shows a scatter plot of a_μ and m_h for a focussed scan with ranges $m_{3/2} \in [0\text{TeV}, 160\text{TeV}]$, $k \in [-0.022, -0.027]$ and $\tan(\beta) \in [2, 12]$. The 2σ region of a_μ is marked with dotted lines while the 2σ region of m_h is marked with dashed lines. The colour denotes the relic density.

Until now, the relic abundance of dark matter has played a pivotal role in assessing the veracity of any given point. However, we find large parts of the parameter space give the right handed stau state as the lightest sparticle. In all preceding plots and in Figure 10 we present results where the neutralino is the LSP. However, it is also interesting to consider potential R-parity violating models in which these light, charged particles decay into standard model particles. Although a detailed discussion of the viability of such points is beyond the scope of this paper, we include Figure 11 as these states can lead to

excellent fits for a_μ and m_h .

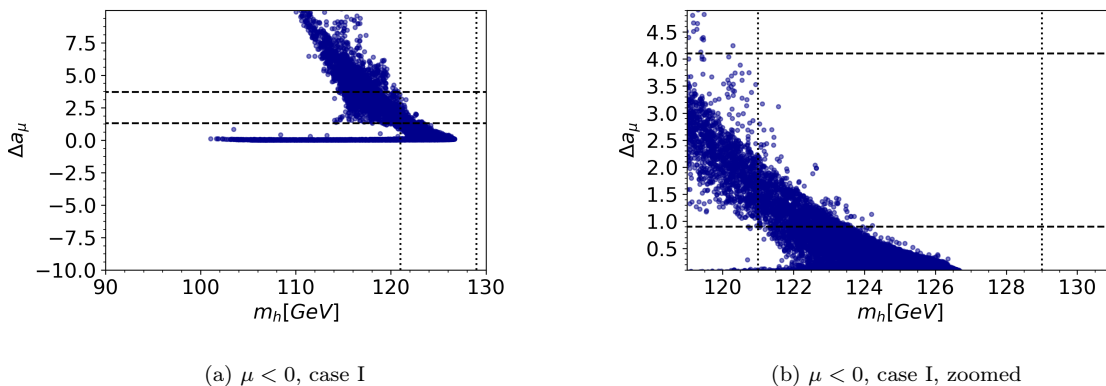


Figure 11: As for Fig 10 but where points that have charged LSP states are shown. Such states are marked in blue to indicate that no relic density could be calculated.

Continuing our analysis, we took a number of points from the allowed region and ran them through CheckMATE. Finding that a sample of points were excluded we wrote a code to systematically check points in the allowed region. We found that all points were either excluded by CheckMATE or in a region near exclusion (allowing for uncertainties in the analysis). We include some of the more promising benchmark points below. It should be noted that we ran CheckMATE using the default 5000 points. However, if a warning was presented speculating that more data could exclude the point in question we increased the number of events by the specified amount.

In Table 9 we present the input parameters for two benchmark points from Case I with negative k values. One point was selected for its relatively high values of Δa_μ whilst the other was selected for its relatively high value of Ωh^2 . Both points are $k = -0.023$ in accordance with the highest likelihood region. Indeed, both points are very similar in a variety of ways suggesting a small input deviations can give large variance in output; particularly for the LSP relic abundance.

Table 10 shows the SUSY spectrum for benchmark points 7 and 8. Strikingly, we see that the lightest stau state is the nLSP behind the usual neutralino LSP. This ofcourse has implications for the most powerful diagrams for the relic density. Furthermore, the nnLSP is given by $\tilde{\mu}_R$ as anticipated by our efforts to generate a high Δa_μ value using diagrams involving this particle. Unlike the sleptons, the squarks are very high in mass contributing to the phenomenologically viable higgs mass. In both cases $\tilde{\tau}_1 - \tilde{\chi}_{10} \approx 10\text{GeV}$. This is important for critical co-annihilation diagrams for the relic density. Again we see that B_0

Quantity	BP7	BP8
α	0	0
β	1	1
$m_{\frac{3}{2}}$ [TeV]	51	57
k	-0.023	-0.023
<u>SPheno:</u>		
m_0 [GeV]	0	0
$\tan(\beta)$	9.72	9.37
$\text{sign}(\mu)$	-1	-1
A_0 [GeV]	0	0
M_1 [GeV]	-263	-263
M_2 [GeV]	-1058	-1152
M_3 [GeV]	-1694	-1863

Table 9: Shows two benchmark points representing two different areas of interest in the parameter space. We present the model parameters and the resultant SPheno input parameters. BP7 shows a point with high a_μ and BP8 shows a point with high Ω . $m_{\frac{3}{2}}$ is given in TeV and all other dimensionful parameters are given in GeV.

is very small in comparison with $m_{\frac{3}{2}}$ suggesting a fully scale-less model.

Both benchmarks produce a completely bino-like LSP state caused by the large scale difference between M_1 and M_2 and have very similar dark matter physics in general. Although BP7 has a dark matter relic density within the allowed region, BP8 gives an excellent value. We see a much larger mass gap between the LSP and the nLSP than for Benchmark points 1 to 6. This is because the points produce a much smaller mass LSP. Therefore, the freeze out temperature is low and as such, there is more cosmological time for co-annihilation to occur. A larger mass gap reduces the strength of these co-annihilation channels allowing for the phenomenological Higgs boson mass.

Table 12 shows some key observables for the given benchmark points. As previously stated, both points are at the borderline of exclusion by Checkmate analysis, since, both points still have relatively low $r_{max} \sim 1$ values, suggesting that both points might be viable within the uncertainties of the analysis, as we discuss further below.

We see short life times for $\tilde{\tau}_1$ with only one decay channel therefore potentially leaving a strong collider signature. Both points get their strongest constraints from the CMS analysis [87] that focuses on direct electroweak production of charginos and neutralinos leading to final state leptons, little hadronic activity, and a large missing momentum.

Masses	BP7	BP8
\tilde{e}_L	661	717
\tilde{e}_R	133	138
$\tilde{\nu}_{eL}$	656	712
$\tilde{\mu}_L$	661	717
$\tilde{\mu}_R$	133	137
$\tilde{\nu}_{\mu L}$	656	712
$\tilde{\tau}_1$	104	109
$\tilde{\tau}_2$	661	717
$\tilde{\nu}_{\tau L}$	654	710
\tilde{d}_L	3110	3390
\tilde{d}_R	3050	3330
\tilde{u}_L	3110	3390
\tilde{u}_R	3050	3320
\tilde{s}_L	3110	3390
\tilde{s}_R	3050	3330
\tilde{c}_L	3110	3390
\tilde{c}_R	3050	3320
\tilde{b}_1	2890	3150
\tilde{b}_2	3040	3310
\tilde{t}_1	2580	2820
\tilde{t}_2	2910	3170
\tilde{g}	3560	3890
$\tilde{\chi}_{10}$	100	99
$\tilde{\chi}_{20}$	855	933
$\tilde{\chi}_{30}$	1890	2060
$\tilde{\chi}_{40}$	1890	2060
$\tilde{\chi}_{1+}$	855	933
$\tilde{\chi}_{2+}$	1890	2060
h_0	121.5	122
H_0	1990	2170
A_0	1990	2170
H_{\pm}	2000	2170
μ	-1777	-1931
B_0	-12	-26.5
$\tilde{\tau}_1 - \tilde{\chi}_{10}$	4.2	9.6

Table 10: Shows the spectrum of SUSY masses for the benchmark points given in Table 9. The difference between the mass of $\tilde{\tau}_1$ and $\tilde{\chi}_{10}$ is also given as this pertains to the production of dark matter. We also include the high scale bilinear coupling value B_0 for its relevance to the high scale parameters of the model. All parameters are given in GeV.

Quantity	BP7	BP8
$\Omega_{DM}h^2$	0.020	0.112
$\tilde{\chi}_{10}$ [GeV]	100	99
$\tilde{\tau}_1 - \tilde{\chi}_{10}$ [GeV]	4.2	9.6
$ \alpha_1 ^2$	1	1
$ \alpha_2 ^2$	0	0
$ \alpha_3 ^2$	0	0
$ \alpha_4 ^2$	0	0

Table 11: Shows the relic density of the LSP for each benchmark point. The difference between the LSP and the nLSP is also given. Finally, we give the probability of finding the given LSP in a particular flavour state. That is to say; we give $|\alpha_i|^2$ where $\tilde{\chi}_{10} = \alpha_1\tilde{B} + \alpha_2\tilde{W} + \alpha_3\tilde{H}_1 + \alpha_4\tilde{H}_2$ and $\sum |\alpha_i|^2 = 1$. Dimensionful parameters are given in GeV.

As the colour charged particles are far more massive than the leptons and gauginos, the latter will represent the dominant production mechanism for the sparticles. The signal region focuses on a final state with three light leptons where two of the three are either e or μ and as we have a light gaugino LSP with light sleptons for $g - 2$ this is likely to be constraining. Furthermore this region focuses on states where the leptonic pair have invariant mass greater than 105GeV and transverse mass of the third lepton greater than 160GeV . $\tilde{\chi}_{20}$ has a 32% branching ratio into $\tilde{\mu}^\pm\mu^\mp / \tilde{e}^\pm e^\mp$ combined with $\tilde{\chi}_{1+}$'s tendency to decay into $\tilde{\tau}\nu_\tau$ pairs creates a strong signal in this region placing the parameter point on the edge of exclusion. Furthermore, the relatively large mass of $\tilde{\chi}_{20}$ means that the resultant lepton pair will exceed the required 105 GeV invariant mass and the production of the τ are on the edge of exclusion of the transverse mass limit. The b-type decays satisfy the experimental constraints for both points.

Quantity	BP7	BP8
$\Gamma_{\tilde{\tau}_1^-}$ [GeV]	3.30×10^{-3}	1.63×10^{-2}
BR ($\tilde{\tau}_1^- \rightarrow \chi_{10} \tau^-$) [%]	100	100
$\Gamma_{\tilde{\mu}_R^-}$ [GeV]	1.32×10^{-1}	1.67×10^{-1}
BR ($\tilde{\mu}_R^- \rightarrow \chi_{10} \mu^-$) [%]	100	100
BR ($b \rightarrow s \gamma$) [%]	0.032	0.032
BR ($B_s \rightarrow \mu^+ \mu^-$) [%]	2.97×10^{-7}	2.96×10^{-7}
$\Delta \frac{(g-2)_\mu}{2}$	1.42×10^{-9}	1.30×10^{-9}
$\Omega_{DM} h^2$	0.020	0.112
χ_{10} [GeV]	100	99
$\sigma_{q\bar{q} \rightarrow \chi_{10} \chi_{10}}$ [pb]	1.796×10^{-14}	3.562×10^{-14}
r_{max}	1.22	1.04
\sqrt{s} [TeV]	13	13
Analysis	cms_sus_16_039	cms_sus_16_039
Signal Region	SR_A44	SR_A44
Ref.	[87]	[87]
σ_{LO} [pb]	7.127×10^{-11}	5.744×10^{-11}

Table 12: Shows branching ratios for lightest supersymmetric particles in the spectrum for BP7 and BP8. Only branching ratio greater than 1% are included. We also include some beyond the standard model observables BR ($b \rightarrow s \gamma$), BR ($B_s \rightarrow \mu^+ \mu^-$), $\Delta \frac{(g-2)_\mu}{2}$, and $\Omega_{DM} h^2$, where $\Delta \frac{(g-2)_\mu}{2}$ is a calculation of the SUSY contribution beyond the standard model. The model successfully predicts the b decays discrepancy and satisfies the anomalous muon magnetic moment to 2σ . The relic density is too small and is therefore not ruled out phenomenologically. CheckMATE runs using 13 TeV and 8 TeV analyses rule out these points. Decay widths and masses are given in GeV, branching ratios are given in %, and cross sections are given in pb.

5 No-scale SUGRA with non-zero A_0 (Case II)

In order to fully explore the parameter space we can also allow for non-zero values of A_0 . Indeed, non-zero A_0 will serve to increase the Higgs boson mass, encouraging a better fit to the current experimental results. We therefore present a subsequent scan where we vary α between -0.016 and 0.016 . These values were chosen by trial and error such that computer time would not be wasted by producing many points with large A_0 values breaking colour charge symmetry.

Analogously to the previous, we start by analysing the positive k values. Further to this analogy, we revert to the previous definition of the likelihood to emphasise the relic density as key constraint in this paradigm and highlight the fact that $g - 2$ will not be satisfied for positive values of k .

5.1 Positive k (Scan 3)

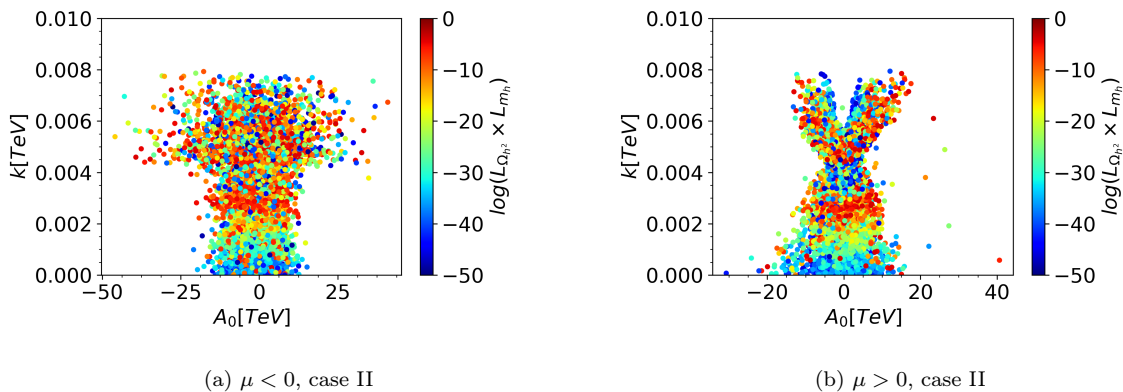


Figure 12: Shows the distribution of A_0 where case I data from a Monte-Carlo scan with parameter ranges $\tan(\beta) \in [1.5, 50]$, $k \in [0, 0.1]$, $\alpha \in [-0.166, 0.166]$, and $m_{\frac{3}{2}} \in [10^3 GeV, 10^6 GeV]$. Colour denotes likelihood, with hotter colours corresponding with high likelihoods. As before, the likelihood is dominated by the relic density calculation.

Fig 12 shows the distribution of A_0 against k for both signs of μ . Interestingly, the shape of the two plots for the two signs of μ is quite different, with the $\mu < 0$ sign yielding a mushroom shaped distribution of points, while the $\mu > 0$ sign results in a wiggam shaped plot. However, there are some key features of both that are shared. In neither do we see any particular likelihood increase for non-0 A_0 . This suggests that moving to case II will

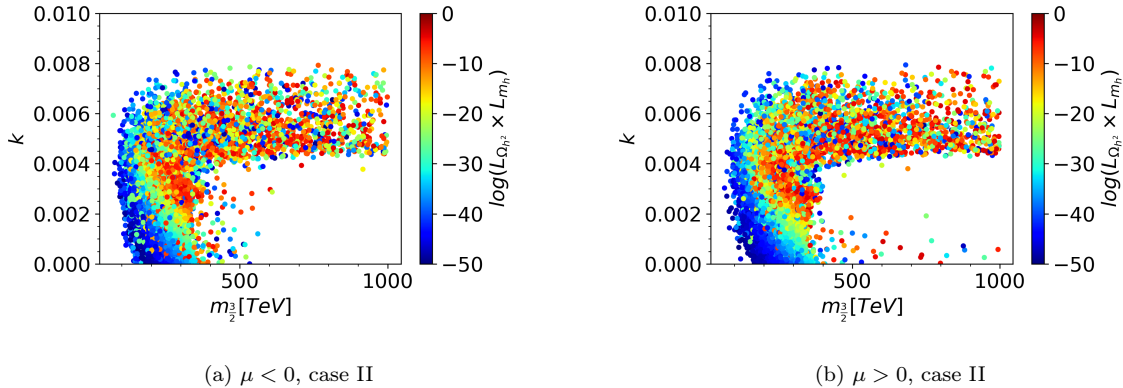


Figure 13: Shows k against $m_{\frac{3}{2}}$ where case II data from a Monte-Carlo scan with parameter ranges $\tan(\beta) \in [1.5, 50]$, $k \in [0, 0.1]$, $\alpha \in [-0.166, 0.166]$, and $m_{\frac{3}{2}} \in [10^3 GeV, 10^6 GeV]$. Colour denotes likelihood, with hotter colours corresponding with high likelihoods. As before, the likelihood is dominated by the relic density calculation.

not give significant improvement compared to the previous case. Furthermore, in both we observe a preferred region of $k \approx 0.003$.

Fig 13 closely mirrors the structure of Fig 7b; with A_0 variation causing some spread in the likelihoods. The structure of LSP make-up as well as spectrum is generally similar. For this reason we refer you to the previous for detailed analysis. Furthermore, the density of points is greatly reduced as variation in A_0 produces many low-likelihood points. This does support claims of naturalness for the exclusively scaleless model previously presented. Although this scan was not truly exhaustive, no gains were made in terms of the overall likelihood.

As in case I with positive k , we see that no point can satisfy the higgs mass and $g - 2$ simultaneously. The same is true of $g - 2$ and the relic density. In order to achieve the correct higgs mass, $m_{\frac{3}{2}}$ must be at least 200TeV. This has the effect of increasing the slepton masses and thus decreasing Δa_μ . We therefore, turn our attention to $k < 0$ values.

5.2 Negative k (Scan 4)

As was previously argued, the inclusion of negative k values should allow for larger Higgs boson masses while keeping slepton masses low; thus incorporating a mechanism for gen-

erating the anomalous muon magnetic moment. As was done previously, we loosen the relic density constraint insisting only that the relic density is sufficiently small so as not to completely rule out the given point. Furthermore, we find large parts of the parameter space give the right handed stau state as the lightest sparticle. In Figures 14 to 16 we present results where the neutralino is the LSP. However, it is also interesting to consider potential R-parity violating models in which these light, charged particles decay into standard model particles. As was previously stated, a detailed discussion of the viability of such points is beyond the scope of this paper, but we do include Figures 17 and 18 as these states can lead to excellent fits for a_μ .

Below we present the results of two scans (over positive and negative μ values). We limit the range of $m_{\frac{3}{2}}$ under the upper limit set by the starobinsky-like inflation limits previously discussed. This eliminates particularly massive gaugino states and thus large slepton mass states.

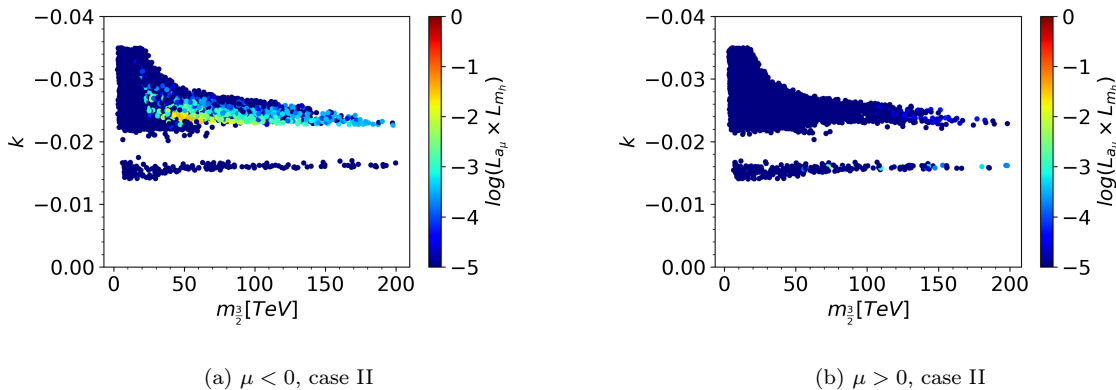


Figure 14: Shows the distribution of k against $m_{\frac{3}{2}}$ with a_μ and m_h log likelihood for $m_{\frac{3}{2}} \in [0\text{TeV}, 200\text{TeV}]$, $\alpha \in [-0.005, 0.005]$ and $k \in [-0.035, -0.014]$.

In both cases, two values of k are favoured by the scan. Analogously to case I, $k \approx -0.016$ and $k \approx -0.0023$ with the latter snf $\mu < 0$ representing a greater likelihood region of parameter space. This gives an approximate ratio of the high scale gaugino mass parameters as $|M_1| : |M_2| : |M_3| \approx 1 : 4 : 7$.

From Fig. 15 and 16 we again see that $\mu < 0$ is favoured with a proportion of points sitting well within the 2σ range. We also observe that some points have a remarkably high relic density almost satisfying the 1σ region. This is a tantalising suggestion that this effectively scaleless model may be able to satisfy the higgs mass, relic density, and a_μ simultaneously. Having said this, the inclusion of A_0 does not give any discernible improvement in the

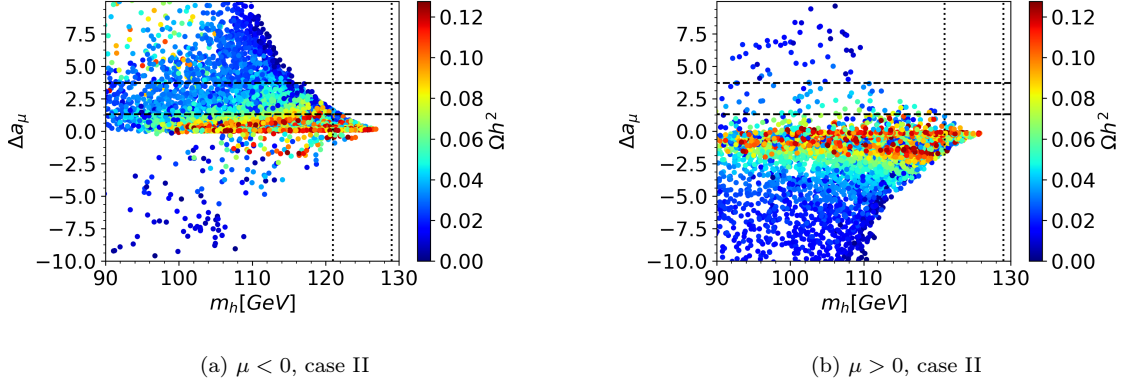


Figure 15: Shows a scatter plot of the higgs mass against the anomalous muon magnetic moment for a scan with ranges $m_{\frac{3}{2}} \in [0TeV, 200TeV]$, $\alpha \in [-0.005, 0.005]$ and $k \in [-0.035, -0.014]$. The 2σ region of a_μ is marked with dotted lines while the 2σ region of m_h is marked with dashed lines. The colour denotes the relic density.

allowed values of the Higgs boson mass due to the previously discussed natural tendency toward a scale-less model. However, these results are still included as the inclusion of a small A_0 parameter can modify the SUSY parameters sufficiently such that some points pass the CheckMATE collider constraints as presented in benchmark points 9 and 10 (Table 13).

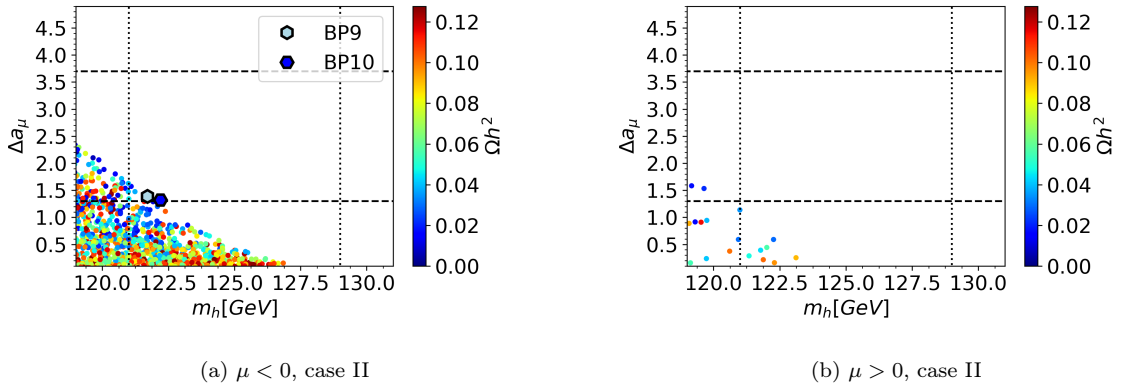


Figure 16: As for Fig 15 but zoomed in on the 3σ region for both a_μ and m_h . Two benchmark points (presented below are marked)

From Fig 17 we can see that allowing for these RPV parameter points slightly increases the a_μ values. Conversely to the previous, $\mu < 0$ now represents the higher likelihood points. As the stau is the lightest particle in the cases, no relic density can be calcu-

lated, and therefore we mark all points in blue to indicate this issue. Having said this, some parameter points perfectly attain the higgs mass and a_μ . For a discussion of the phenomenology of such points see [60].

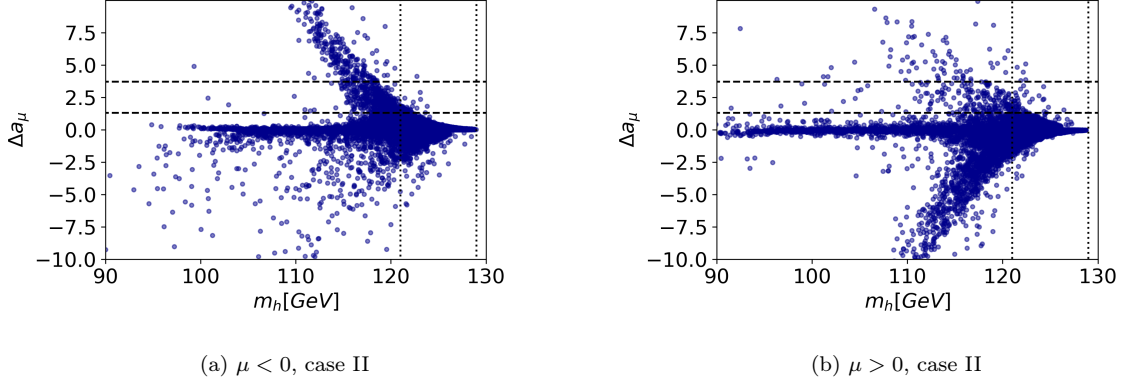


Figure 17: As for Fig 15 but where points that have charged LSP states are shown. Such states are marked in blue to indicate that no relic density could be calculated.

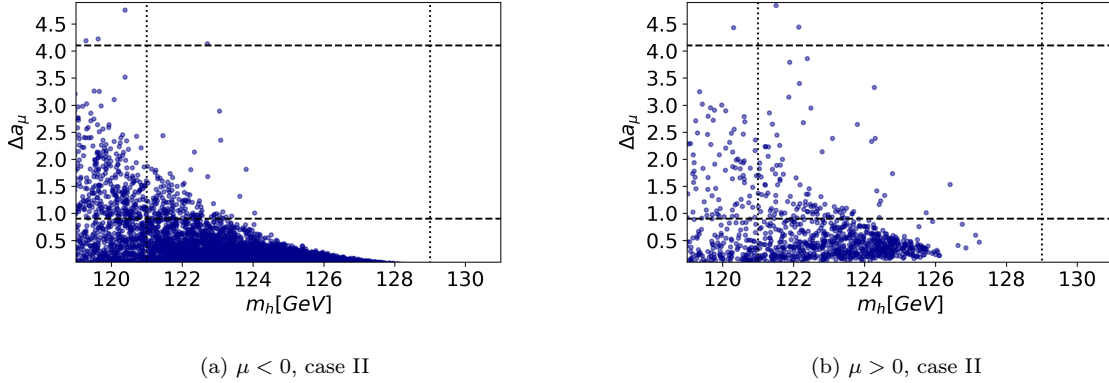


Figure 18: As for Fig 17 but zoomed in on the 3σ region for both a_μ and m_h .

We now present the two benchmark points plotted on Fig 16. Both were selected to represent a particularly high value of a_μ as well as interesting collider results.

Both benchmarks 9,10 have the same value of k as shown in Fig 12 where $k = -0.23$ had clear phenomenological advantages. Furthermore, the values of $m_{\frac{3}{2}}$ and $\tan(\beta)$ are also approximately similar. They are both selected from the $\mu < 0$ scan due to its more promising phenomenology. In both cases $\beta \approx 1$ and α is very small. This is consistent with the no-scale model we are examining. The high scale gaugino mass parameters are

also presented. After running to the low scale the ratio becomes far more extreme causing a great hierarchical divergence between the colour charged and the non-colour charged sparticles as can be seen below.

Table 14 shows the mass spectrum for the two benchmark points BP9, BP10. Large values of M_3 give large values of squark and gluon masses and contribute to the relatively large higgs mass. Conversely, the smaller values of the other two gaugino mass parameters, in combination with the absence of m_0 , gives the requisite small slepton states. Furthermore, the hierarchy between M_1 and M_2 gives a notable disparity between the right and left handed states. Due to the small value of $\tan(\beta)$ and the negative sign of μ , $\tilde{\tau}_1$ is predominantly right handed. We note the very light smuon states that give key contributions to a_μ . Finally, the small value of M_1 leads to predominantly bino-like, light dark matter candidate.

Table 15 shows the key parameters for the relic density calculation for the two points BP9, BP10. As the stau is the nLSP, the mass difference between it and $\tilde{\chi}_{10}$ is presented. As its mass gap is so small, the $\tilde{\tau}$ plays a critical role in the mechanism for dark matter annihilation. Indeed the dominant decay channels contributing to the relic density calculation are $\tilde{\tau}_1 \tilde{\tau}_1 \rightarrow \tau \tau$ and $\tilde{\tau}_1 \tilde{\chi}_{10} \rightarrow \tau \gamma$. As the mass gap is especially small in the BP9, dark matter is over-annihilated by these channels leading to a relic density below the desired value.

Table 16 shows the key collider and phenomenological findings resulting from these parameter points BP9, BP10. Both the nnLSP, $\tilde{\mu}_R$, and the LSP $\tilde{\tau}_1$, have short lifetimes with only one decay channel perhaps suggesting a strong collider signature. Indeed, the strongest signal region for both BP9 and BP10 is one that focuses on dileptonic final states with missing transverse energy in the context of "electroweakinos". Both b-type branching ratios are very well fitted in both cases. Furthermore, a_μ is within the 2σ region for BP9 and BP10. We see relatively high values of r calculated by CheckMATE due to the low mass sleptons.

Quantity	BP9	BP10
α	0.0007	0.0003
β	1	1
$m_{\frac{3}{2}}$ [TeV]	56	57
k	-0.023	-0.023
<u>SPheno:</u>		
m_0 [GeV]	0	0
$\tan(\beta)$	10.5	10.0
$\text{sign}(\mu)$	-1	-1
A_0 [GeV]	-227	-109
M_1 [GeV]	-275	-271
M_2 [GeV]	-1144	-1163
M_3 [GeV]	-1841	-1877

Table 13: Shows two benchmark points representing two different areas of interest in the parameter space. We present the model parameters and the resultant SPheno input parameters. BP9 shows a point with high a_μ and BP10 shows a point with high Ω . Dimensions of the parameters are given where "-" means dimensionless. $m_{\frac{3}{2}}$ is given in units of TeV, and m_0, A_0, M_i are given in GeV.

Masses	BP9	BP10
\tilde{e}_L	712	724
\tilde{e}_R	139	140
$\tilde{\nu}_{eL}$	708	719
$\tilde{\mu}_L$	712	724
$\tilde{\mu}_R$	139	140
$\tilde{\nu}_{\mu L}$	708	719
$\tilde{\tau}_1$	107	110
$\tilde{\tau}_2$	712	724
$\tilde{\nu}_{\tau L}$	706	717
\tilde{d}_L	3360	3420
\tilde{d}_R	3290	3350
\tilde{u}_L	3360	3420
\tilde{u}_R	3290	3350
\tilde{s}_L	3360	3420
\tilde{s}_R	3290	3350
\tilde{c}_L	3360	3420
\tilde{c}_R	3290	3350
\tilde{b}_1	3120	3180
\tilde{b}_2	3280	3340
\tilde{t}_1	2800	2840
\tilde{t}_2	3140	3190
\tilde{g}	3850	3920
$\tilde{\chi}_{10}$	103	103
$\tilde{\chi}_{20}$	926	942
$\tilde{\chi}_{30}$	2000	2050
$\tilde{\chi}_{40}$	2000	2060
$\tilde{\chi}_{1+}$	926	943
$\tilde{\chi}_{2+}$	2009	2060
h_0	122	122
H_0	2110	2160
A_0	2110	2160
H_{\pm}	2110	2170
μ	-1870	-1930
B_0	-68	-46
$\tilde{\tau}_1 - \tilde{\chi}_{10}$	3.87	6.77

Table 14: Shows the spectrum of SUSY masses for the benchmark points given in Table 13. The difference between the mass of $\tilde{\tau}_1$ and $\tilde{\chi}_{10}$ is also given as this pertains to the production of dark matter. We also include the high scale bilinear coupling value B_0 for its relevance to the high scale parameters of the model. All parameters are given in GeV.

Quantity	BP9	BP10
$\Omega_{DM}h^2$	0.0397	0.020
$\tilde{\chi}_{10}$ [GeV]	103	103
$\tilde{\tau}_1 - \tilde{\chi}_{10}$ [GeV]	3.87	6.77
$ \alpha_1 ^2$	1	1
$ \alpha_2 ^2$	0	0
$ \alpha_3 ^2$	0	0
$ \alpha_4 ^2$	0	0

Table 15: Shows the relic density of the LSP for each benchmark point. The difference between the LSP and the nLSP is also given. Finally, we give the probability of finding the LSP in a particular flavour state. That is to say; we give $|\alpha_i|^2$ where $\tilde{\chi}_{10} = \alpha_1\tilde{B} + \alpha_2\tilde{W} + \alpha_3\tilde{H}_1 + \alpha_4\tilde{H}_2$ and $\sum |\alpha_i|^2 = 1$. Dimensionful parameters are given in GeV.

Quantity	BP9	BP10
$\Gamma_{\tilde{\tau}_1}$ [Gev]	2.61×10^{-3}	8.18×10^{-3}
BR ($\tilde{\tau}_1^- \rightarrow \chi_{10} \tau^-$) [%]	100	100
$\Gamma_{\tilde{\mu}_R}$ [Gev]	1.47×10^{-1}	1.57×10^{-1}
BR ($\tilde{\mu}_R^- \rightarrow \chi_{10} \mu^-$) [%]	100	100
BR ($b \rightarrow s \gamma$) [%]	0.032	0.032
BR ($B_s \rightarrow \mu^+ \mu^-$) [%]	2.96×10^{-7}	2.95×10^{-7}
$\Delta_{\frac{(g-2)_\mu}{2}}$	1.39×10^{-9}	1.32×10^{-9}
$\Omega_{DM} h^2$	0.0397	0.020
χ_{10} [Gev]	103	103
$\sigma_{q\bar{q} \rightarrow \chi_{10} \chi_{10}}$ [pb]	3.982×10^{-14}	2.290×10^{-14}
r_{max}	0.40	0.57
\sqrt{s} [TeV]	13	13
Analysis	cms_sus_16_039	cms_sus_16_039
Signal Region	SR_A44	SR_A44
Ref.	[87]	[87]
σ_{LO} [pb]	6.342×10^{-11}	5.893×10^{-11}

Table 16: Shows branching ratios for lightest supersymmetric particles in the spectrum for BP7 and BP8. Only branching ratio greater than 1% are included. We also include some beyond the standard model observables BR ($b \rightarrow s \gamma$), BR ($B_s \rightarrow \mu^+ \mu^-$), $\Delta_{\frac{(g-2)_\mu}{2}}$, and $\Omega_{DM} h^2$, where $\Delta_{\frac{(g-2)_\mu}{2}}$ is a calculation of the SUSY contribution beyond the standard model. The model successfully predicts the b decays discrepancy and satisfies the anomalous muon magnetic moment to $2/3\sigma$. The relic density is too small and is therefore not ruled out phenomenologically. CheckMATE runs using 13TeV and 8TeV analyses do not rule out these points. Decay widths and masses are given in GeV, branching ratios are given in %, and cross sections are given in pb.

6 Conclusion

Inflation represents a very attractive solution to a number of cosmological problems and, in combination with supersymmetry, a very attractive model for Beyond the Standard Model physics emerges based on no-scale SUGRA. We have focussed on the particular case where the Polonyi term in the superpotential acts as a slow roll inflaton for Starobinsky inflation, leading to an upper bound on the gravitino mass $m_{3/2} < 1000$ TeV.

The recent Fermilab muon $g - 2$ result further motivates a no-scale model, where all the dimensionful parameters the model are zero (except the gaugino masses which arise via mixed modulus and anomaly mediation), naturally leading to light slepton masses for certain gaugino masses. For negative universal gaugino masses, $k < 0$, we find relatively light bino/wino masses together with light sleptons, as suggested by the muon $g - 2$ measurement. In general, such a model is also capable of providing a good dark matter candidate whilst satisfying constraints from collider physics, as well as yielding the correct Higgs boson mass, but it turns out to be non-trivial to achieve this while satisfying the desired muon $g - 2$ constraints.

We have conducted a Monte Carlo parameter scan over the given model in two conditions: case I and case II, corresponding to zero or non-zero trilinear soft parameter A_0 . We show that case I with $k > 0$ can give excellent fits for the Higgs boson mass and relic density whilst easily satisfying the collider and flavour constraints. Furthermore, with a reversal in the sign of k we show that $g - 2$ can be satisfied to 2σ , as exemplified by BP7 and BP8, where BP8 also satisfies the desired relic density. Since BP7 and BP8 are on the edge of exclusion, with r_{max} values slightly above unity, this motivates the study of case II where we allow a non-zero A_0 trilinear soft parameter. By including a small A_0 parameter at the high scale, we find that muon $g - 2$ can be satisfied whilst satisfying the collider constraints that threaten case I. However we find, while the case II benchmark points BP9 and BP10 satisfy the collider constraints and the muon $g - 2$, they both predict a relic density which is below the desired value, which does not exclude these points of course, but is somewhat disappointing from the point of view of dark matter. Interestingly, we find that, in both cases, a large part of parameter space is dominated by RPV-style points, where the LSP becomes the lightest $\tilde{\tau}$ state. Although such states are beyond the scope of this paper, a detailed discussion of these kind of points can be found [60].

In general, we find that the lightest neutralino $\tilde{\chi}_{10}$ should be a purely bino-like state with a mass of around 100 GeV for parameter points BP7-BP10 that satisfy the muon $g - 2$ constraint. We highlight in particular the fully no-scale SUGRA point with zero

A_0 , B_0 and m_0 , namely BP8, which can explain not only the recent Fermilab muon $g - 2$ measurement, and has the correct Higgs boson mass, but also yields the desired dark matter relic density, albeit with $r_{max} = 1.04$ on the edge of exclusion. We remark that current LHC limits are more easily evaded due to right handed sleptons being almost degenerate with the neutralino LSP, while the left handed counterparts are much higher in mass, suppressing chargino decay channels into first and second generation sleptons. However, even for BP9 and BP10, the r_{max} value is not too far from unity, suggesting that future LHC runs are capable of discovering such SUSY particles for all the interesting benchmarks that satisfy the muon $g - 2$.

In conclusion, no-scale SUGRA is not only well motivated theoretically from string theory and provides an elegant framework for accounting for cosmological Starobinsky inflation, but also has very interesting phenomenological implications as well. Ignoring the muon $g - 2$ to begin with, and assuming positive universal gaugino mass contributions, in addition to the anomaly mediated contributions, we show that no-scale SUGRA can readily satisfy the dark matter and Higgs boson mass requirements, consistently with all other phenomenological constraints. We then show that the recent Fermilab measurement of the muon $g - 2$ may be accommodated, together with the correct Higgs boson mass, for no-scale SUGRA with negative universal gaugino mass contributions in addition to the anomaly mediated contributions. For the fully no-scale SUGRA case, with all soft parameters equal to zero at the high scale, apart from gaugino masses, we find that successful points which satisfy the muon $g - 2$, and can sometimes yield the desired relic density, although such points tend to be near the edge of LHC collider exclusion. Analysing no-scale SUGRA with a non-zero A_0 , we find that the muon $g - 2$ can still be explained, with the collider constraints somewhat relaxed. However, even in this case, light sleptons and charginos are still predicted, with good prospects for discovering these SUSY particles in LHC Run 3.

7 Acknowledgments

The authors acknowledge the use of the IRIDIS High Performance Computing Facility, and associated support services at the University of Southampton, in the completion of this work. SFK acknowledges the STFC Consolidated Grant ST/L000296/1 and the European Union's Horizon 2020 Research and Innovation programme under Marie Skłodowska-Curie grant agreement HIDDeN European ITN project (H2020-MSCA-ITN-2019//860881-HIDDeN).

References

- [1] G. W. Bennett *et al.* [Muon $g-2$], Phys. Rev. D **73** (2006), 072003 doi:10.1103/PhysRevD.73.072003 [arXiv:hep-ex/0602035 [hep-ex]].
- [2] B. Abi *et al.* [Muon $g-2$], Phys. Rev. Lett. **126** (2021) no.14, 141801 doi:10.1103/PhysRevLett.126.141801 [arXiv:2104.03281 [hep-ex]].
- [3] T. Aoyama, N. Asmussen, M. Benayoun, J. Bijnens, T. Blum, M. Bruno, I. Caprini, C. M. Carloni Calame, M. Cè and G. Colangelo, *et al.* Phys. Rept. **887** (2020), 1-166 doi:10.1016/j.physrep.2020.07.006 [arXiv:2006.04822 [hep-ph]].
- [4] T. Aoyama, M. Hayakawa, T. Kinoshita and M. Nio, Phys. Rev. Lett. **109** (2012), 111808 doi:10.1103/PhysRevLett.109.111808 [arXiv:1205.5370 [hep-ph]].
- [5] T. Aoyama, T. Kinoshita and M. Nio, Atoms **7** (2019) no.1, 28 doi:10.3390/atoms7010028
- [6] A. Czarnecki, W. J. Marciano and A. Vainshtein, Phys. Rev. D **67** (2003), 073006 [erratum: Phys. Rev. D **73** (2006), 119901] doi:10.1103/PhysRevD.67.073006 [arXiv:hep-ph/0212229 [hep-ph]].
- [7] C. Gnendiger, D. Stöckinger and H. Stöckinger-Kim, Phys. Rev. D **88** (2013), 053005 doi:10.1103/PhysRevD.88.053005 [arXiv:1306.5546 [hep-ph]].
- [8] M. Davier, A. Hoecker, B. Malaescu and Z. Zhang, Eur. Phys. J. C **77** (2017) no.12, 827 doi:10.1140/epjc/s10052-017-5161-6 [arXiv:1706.09436 [hep-ph]].
- [9] A. Keshavarzi, D. Nomura and T. Teubner, Phys. Rev. D **97** (2018) no.11, 114025 doi:10.1103/PhysRevD.97.114025 [arXiv:1802.02995 [hep-ph]].
- [10] G. Colangelo, M. Hoferichter and P. Stoffer, JHEP **02** (2019), 006 doi:10.1007/JHEP02(2019)006 [arXiv:1810.00007 [hep-ph]].
- [11] M. Hoferichter, B. L. Hoid and B. Kubis, JHEP **08** (2019), 137 doi:10.1007/JHEP08(2019)137 [arXiv:1907.01556 [hep-ph]].
- [12] M. Davier, A. Hoecker, B. Malaescu and Z. Zhang, Eur. Phys. J. C **80** (2020) no.3, 241 [erratum: Eur. Phys. J. C **80** (2020) no.5, 410] doi:10.1140/epjc/s10052-020-7792-2 [arXiv:1908.00921 [hep-ph]].
- [13] A. Keshavarzi, D. Nomura and T. Teubner, Phys. Rev. D **101** (2020) no.1, 014029 doi:10.1103/PhysRevD.101.014029 [arXiv:1911.00367 [hep-ph]].
- [14] A. Kurz, T. Liu, P. Marquard and M. Steinhauser, Phys. Lett. B **734** (2014), 144-147 doi:10.1016/j.physletb.2014.05.043 [arXiv:1403.6400 [hep-ph]].

- [15] K. Melnikov and A. Vainshtein, *Phys. Rev. D* **70** (2004), 113006 doi:10.1103/PhysRevD.70.113006 [arXiv:hep-ph/0312226 [hep-ph]].
- [16] P. Masjuan and P. Sanchez-Puertas, *Phys. Rev. D* **95** (2017) no.5, 054026 doi:10.1103/PhysRevD.95.054026 [arXiv:1701.05829 [hep-ph]].
- [17] G. Colangelo, M. Hoferichter, M. Procura and P. Stoffer, *JHEP* **04** (2017), 161 doi:10.1007/JHEP04(2017)161 [arXiv:1702.07347 [hep-ph]].
- [18] M. Hoferichter, B. L. Hoid, B. Kubis, S. Leupold and S. P. Schneider, *JHEP* **10** (2018), 141 doi:10.1007/JHEP10(2018)141 [arXiv:1808.04823 [hep-ph]].
- [19] A. Gérardin, H. B. Meyer and A. Nyffeler, *Phys. Rev. D* **100** (2019) no.3, 034520 doi:10.1103/PhysRevD.100.034520 [arXiv:1903.09471 [hep-lat]].
- [20] J. Bijnens, N. Hermansson-Truedsson and A. Rodríguez-Sánchez, *Phys. Lett. B* **798** (2019), 134994 doi:10.1016/j.physletb.2019.134994 [arXiv:1908.03331 [hep-ph]].
- [21] G. Colangelo, F. Hagelstein, M. Hoferichter, L. Laub and P. Stoffer, *JHEP* **03** (2020), 101 doi:10.1007/JHEP03(2020)101 [arXiv:1910.13432 [hep-ph]].
- [22] T. Blum, N. Christ, M. Hayakawa, T. Izubuchi, L. Jin, C. Jung and C. Lehner, *Phys. Rev. Lett.* **124** (2020) no.13, 132002 doi:10.1103/PhysRevLett.124.132002 [arXiv:1911.08123 [hep-lat]].
- [23] G. Colangelo, M. Hoferichter, A. Nyffeler, M. Passera and P. Stoffer, *Phys. Lett. B* **735** (2014), 90-91 doi:10.1016/j.physletb.2014.06.012 [arXiv:1403.7512 [hep-ph]].
- [24] A. Czarnecki and W. J. Marciano, *Phys. Rev. D* **64** (2001), 013014 doi:10.1103/PhysRevD.64.013014 [arXiv:hep-ph/0102122 [hep-ph]].
- [25] Q. Shafi and C. S. Ün, [arXiv:2107.04563 [hep-ph]].
- [26] S. M. Zhao, L. H. Su, X. X. Dong, T. T. Wang and T. F. Feng, [arXiv:2107.03571 [hep-ph]].
- [27] Z. Li, G. L. Liu, F. Wang, J. M. Yang and Y. Zhang, [arXiv:2106.04466 [hep-ph]].
- [28] F. Wang, L. Wu, Y. Xiao, J. M. Yang and Y. Zhang, *Nucl. Phys. B* **970** (2021), 115486 doi:10.1016/j.nuclphysb.2021.115486 [arXiv:2104.03262 [hep-ph]].
- [29] Y. Gu, N. Liu, L. Su and D. Wang, *Nucl. Phys. B* **969** (2021), 115481 doi:10.1016/j.nuclphysb.2021.115481 [arXiv:2104.03239 [hep-ph]].
- [30] C. Han, [arXiv:2104.03292 [hep-ph]].
- [31] M. Endo, K. Hamaguchi, S. Iwamoto and T. Kitahara, *JHEP* **04** (2020), 165 doi:10.1007/JHEP04(2020)165 [arXiv:2001.11025 [hep-ph]].
- [32] J. Cao, J. Lian, Y. Pan, D. Zhang and P. Zhu, [arXiv:2104.03284 [hep-ph]].

- [33] A. B. Lahanas and D. V. Nanopoulos, Phys. Rept. **145** (1987), 1 doi:10.1016/0370-1573(87)90034-2
- [34] A. H. Guth, Phys. Rev. D **23** (1981), 347-356 doi:10.1103/PhysRevD.23.347
- [35] A. D. Linde, Phys. Lett. B **108** (1982), 389-393 doi:10.1016/0370-2693(82)91219-9
- [36] V. F. Mukhanov and G. V. Chibisov, JETP Lett. **33** (1981), 532-535
- [37] A. Albrecht and P. J. Steinhardt, Phys. Rev. Lett. **48** (1982), 1220-1223 doi:10.1103/PhysRevLett.48.1220
- [38] A. D. Linde, Phys. Lett. B **129** (1983), 177-181 doi:10.1016/0370-2693(83)90837-7
- [39] A. D. Linde, Lect. Notes Phys. **738** (2008), 1-54 doi:10.1007/978-3-540-74353-8_1 [arXiv:0705.0164 [hep-th]].
- [40] A. D. Linde, Contemp. Concepts Phys. **5** (1990), 1-362 [arXiv:hep-th/0503203 [hep-th]].
- [41] D. H. Lyth and A. Riotto, Phys. Rept. **314** (1999), 1-146 doi:10.1016/S0370-1573(98)00128-8 [arXiv:hep-ph/9807278 [hep-ph]].
- [42] P. A. R. Ade *et al.* [Planck], Astron. Astrophys. **594** (2016), A20 doi:10.1051/0004-6361/201525898 [arXiv:1502.02114 [astro-ph.CO]].
- [43] J. Martin, C. Ringeval and V. Vennin, Phys. Dark Univ. **5-6** (2014), 75-235 doi:10.1016/j.dark.2014.01.003 [arXiv:1303.3787 [astro-ph.CO]].
- [44] A. A. Starobinsky, Phys. Lett. B **91** (1980), 99-102 doi:10.1016/0370-2693(80)90670-X
- [45] J. R. Ellis, D. V. Nanopoulos, K. A. Olive and K. Tamvakis, Phys. Lett. B **120** (1983), 331-334 doi:10.1016/0370-2693(83)90456-2
- [46] J. R. Ellis, D. V. Nanopoulos, K. A. Olive and K. Tamvakis, Phys. Lett. B **118** (1982), 335 doi:10.1016/0370-2693(82)90198-8
- [47] J. R. Ellis, D. V. Nanopoulos, K. A. Olive and K. Tamvakis, Nucl. Phys. B **221** (1983), 524-548 doi:10.1016/0550-3213(83)90592-8
- [48] J. R. Ellis, K. Enqvist, D. V. Nanopoulos, K. A. Olive and M. Srednicki, Phys. Lett. B **152** (1985), 175 [erratum: Phys. Lett. B **156** (1985), 452] doi:10.1016/0370-2693(85)91164-5
- [49] S. Antusch, M. Bastero-Gil, K. Dutta, S. F. King and P. M. Kostka, Phys. Lett. B **679** (2009), 428-432 doi:10.1016/j.physletb.2009.08.022 [arXiv:0905.0905 [hep-th]].
- [50] S. Antusch and F. Cefalà, JCAP **10** (2013), 055 doi:10.1088/1475-7516/2013/10/055 [arXiv:1306.6825 [hep-ph]].

- [51] K. Nakayama, F. Takahashi and T. T. Yanagida, Phys. Lett. B **725** (2013), 111-114 doi:10.1016/j.physletb.2013.06.050 [arXiv:1303.7315 [hep-ph]].
- [52] S. C. Davis and M. Postma, JCAP **03** (2008), 015 doi:10.1088/1475-7516/2008/03/015 [arXiv:0801.4696 [hep-ph]].
- [53] R. Kallosh, A. Linde, K. A. Olive and T. Rube, Phys. Rev. D **84** (2011), 083519 doi:10.1103/PhysRevD.84.083519 [arXiv:1106.6025 [hep-th]].
- [54] D. H. Lyth, Phys. Lett. B **147** (1984), 403 [erratum: Phys. Lett. B **150** (1985), 465] doi:10.1016/0370-2693(84)91391-1
- [55] J. Ellis, D. V. Nanopoulos and K. A. Olive, Phys. Rev. Lett. **111** (2013), 111301 [erratum: Phys. Rev. Lett. **111** (2013) no.12, 129902] doi:10.1103/PhysRevLett.111.111301 [arXiv:1305.1247 [hep-th]].
- [56] J. Ellis, D. V. Nanopoulos and K. A. Olive, JCAP **10** (2013), 009 doi:10.1088/1475-7516/2013/10/009 [arXiv:1307.3537 [hep-th]].
- [57] J. Ellis, D. V. Nanopoulos and K. A. Olive, Phys. Rev. D **89** (2014) no.4, 043502 doi:10.1103/PhysRevD.89.043502 [arXiv:1310.4770 [hep-ph]].
- [58] M. C. Romao and S. F. King, JHEP **07** (2017), 033 doi:10.1007/JHEP07(2017)033 [arXiv:1703.08333 [hep-ph]].
- [59] S. F. King and E. Perdomo, JHEP **05** (2019), 211 doi:10.1007/JHEP05(2019)211 [arXiv:1903.08448 [hep-ph]].
- [60] K. S. Jeong, J. Kawamura and C. B. Park, [arXiv:2106.04238 [hep-ph]].
- [61] W. Porod, Comput. Phys. Commun. **153** (2003), 275-315 doi:10.1016/S0010-4655(03)00222-4 [arXiv:hep-ph/0301101 [hep-ph]].
- [62] W. Porod and F. Staub, Comput. Phys. Commun. **183** (2012), 2458-2469 doi:10.1016/j.cpc.2012.05.021 [arXiv:1104.1573 [hep-ph]].
- [63] S. Heinemeyer, W. Hollik and G. Weiglein, Comput. Phys. Commun. **124** (2000), 76-89 doi:10.1016/S0010-4655(99)00364-1 [arXiv:hep-ph/9812320 [hep-ph]].
- [64] G. Belanger, F. Boudjema, A. Pukhov and A. Semenov, Comput. Phys. Commun. **174** (2006), 577-604 doi:10.1016/j.cpc.2005.12.005 [arXiv:hep-ph/0405253 [hep-ph]].
- [65] G. Belanger, F. Boudjema, A. Pukhov and A. Semenov, Comput. Phys. Commun. **176** (2007), 367-382 doi:10.1016/j.cpc.2006.11.008 [arXiv:hep-ph/0607059 [hep-ph]].
- [66] G. Belanger, F. Boudjema, A. Pukhov and A. Semenov, Comput. Phys. Commun. **180** (2009), 747-767 doi:10.1016/j.cpc.2008.11.019 [arXiv:0803.2360 [hep-ph]].

- [67] G. Belanger, F. Boudjema, A. Pukhov and A. Semenov, *Nuovo Cim. C* **033N2** (2010), 111-116 doi:10.1393/ncc/i2010-10591-3 [arXiv:1005.4133 [hep-ph]].
- [68] G. Belanger, F. Boudjema, A. Pukhov and A. Semenov, *Comput. Phys. Commun.* **185** (2014), 960-985 doi:10.1016/j.cpc.2013.10.016 [arXiv:1305.0237 [hep-ph]].
- [69] M. Drees, H. Dreiner, D. Schmeier, J. Tattersall and J. S. Kim, *Comput. Phys. Commun.* **187** (2015), 227-265 doi:10.1016/j.cpc.2014.10.018 [arXiv:1312.2591 [hep-ph]].
- [70] D. Dercks, N. Desai, J. S. Kim, K. Rolbiecki, J. Tattersall and T. Weber, *Comput. Phys. Commun.* **221** (2017), 383-418 doi:10.1016/j.cpc.2017.08.021 [arXiv:1611.09856 [hep-ph]].
- [71] J. L. Evans, N. Nagata and K. A. Olive, *Eur. Phys. J. C* **79** (2019) no.6, 490 doi:10.1140/epjc/s10052-019-6980-4 [arXiv:1902.09084 [hep-ph]].
- [72] K. S. Jeong, J. Kawamura and C. B. Park, [arXiv:2106.04238 [hep-ph]].
- [73] J. R. Ellis, K. A. Olive, Y. Santoso and V. C. Spanos, *Phys. Rev. D* **70** (2004), 055005 doi:10.1103/PhysRevD.70.055005 [arXiv:hep-ph/0405110 [hep-ph]].
- [74] W. K. Hastings, *Biometrika* **57** (1970), 97-109 doi:10.1093/biomet/57.1.97
- [75] J. Ellis, J. L. Evans, N. Nagata, K. A. Olive and L. Velasco-Sevilla, *Eur. Phys. J. C* **81** (2021) no.2, 120 doi:10.1140/epjc/s10052-021-08903-5 [arXiv:2011.03554 [hep-ph]].
- [76] R. Frederix, S. Frixione, V. Hirschi, D. Pagani, H. S. Shao and M. Zaro, *JHEP* **07** (2018), 185 doi:10.1007/JHEP07(2018)185 [arXiv:1804.10017 [hep-ph]].
- [77] J. Alwall, R. Frederix, S. Frixione, V. Hirschi, F. Maltoni, O. Mattelaer, H. S. Shao, T. Stelzer, P. Torrielli and M. Zaro, *JHEP* **07** (2014), 079 doi:10.1007/JHEP07(2014)079 [arXiv:1405.0301 [hep-ph]].
- [78] T. Sjöstrand, S. Ask, J. R. Christiansen, R. Corke, N. Desai, P. Ilten, S. Mrenna, S. Prestel, C. O. Rasmussen and P. Z. Skands, *Comput. Phys. Commun.* **191** (2015), 159-177 doi:10.1016/j.cpc.2015.01.024 [arXiv:1410.3012 [hep-ph]].
- [79] T. Sjostrand, S. Mrenna and P. Z. Skands, *Comput. Phys. Commun.* **178** (2008), 852-867 doi:10.1016/j.cpc.2008.01.036 [arXiv:0710.3820 [hep-ph]].
- [80] J. de Favereau *et al.* [DELPHES 3], *JHEP* **02** (2014), 057 doi:10.1007/JHEP02(2014)057 [arXiv:1307.6346 [hep-ex]].
- [81] M. Cacciari and G. P. Salam, *Phys. Lett. B* **641** (2006), 57-61 doi:10.1016/j.physletb.2006.08.037 [arXiv:hep-ph/0512210 [hep-ph]].
- [82] M. Cacciari, G. P. Salam and G. Soyez, *Eur. Phys. J. C* **72** (2012), 1896 doi:10.1140/epjc/s10052-012-1896-2 [arXiv:1111.6097 [hep-ph]].

- [83] M. Cacciari, G. P. Salam and G. Soyez, JHEP **04** (2008), 063 doi:10.1088/1126-6708/2008/04/063 [arXiv:0802.1189 [hep-ph]].
- [84] A. L. Read, J. Phys. G **28** (2002), 2693-2704 doi:10.1088/0954-3899/28/10/313
- [85] M. Aaboud *et al.* [ATLAS], JHEP **01** (2018), 126 doi:10.1007/JHEP01(2018)126 [arXiv:1711.03301 [hep-ex]].
- [86] G. Aad *et al.* [ATLAS], JHEP **02** (2021), 143 doi:10.1007/JHEP02(2021)143 [arXiv:2010.14293 [hep-ex]].
- [87] A. M. Sirunyan *et al.* [CMS], JHEP **03** (2018), 166 doi:10.1007/JHEP03(2018)166 [arXiv:1709.05406 [hep-ex]].